



Mechanism of the historical and the ongoing Vulcanian eruptions of Ebeko volcano, Northern Kuriles

A. Belousov¹ · M. Belousova¹ · A. Auer² · T. R. Walter³ · T. Kotenko¹

Received: 18 August 2020 / Accepted: 1 December 2020

© International Association of Volcanology & Chemistry of the Earth's Interior 2021

Abstract

Ebeko is one of the most active volcanoes of the Kurile island arc, producing frequent mild Vulcanian explosions with eruption clouds up to 5 km high. The volcano poses a serious threat to the Severo-Kurilsk town with a population of around 2500 inhabitants, located at a distance of only 7 km on a fan of the volcano's laharic deposits. Here, we report an overview of the activity of the volcano in the 20th–21st centuries and the results of our geological and petrological investigations of the ongoing Vulcanian eruption that started in 2016. We have found that eruptions of Ebeko span a range of mechanisms from purely magmatic to phreatic/hydrothermal. Three of its historical eruptions (the 1934–1935, 1987–1991, and the 2016–ongoing) involved fresh magma, while during the others (1967–1971, 2009–2011) fresh magma was not erupted. Juvenile material of the ongoing eruption represents highly crystalline and highly viscous (more than 10^8 pa s) low-silica (56–58 wt% SiO₂) andesite. Historical data and our observations of the ongoing eruption allowed us to suggest a functional model of the volcano where Vulcanian explosions are caused by shallow intrusions of small diapir-like batches of strongly crystallized and highly viscous andesitic magma ascending into water-saturated, hydrothermally altered rocks composing the volcano summit. We suggest that the diapir's ascent is governed by their positive buoyancy. Some of the diapirs reach and breach the ground surface producing magmatic eruptions of Ebeko, while the others are stuck at the shallow subsurface level and feed intensive hydrothermal activity as well as phreatic eruptions of the volcano. Positive buoyancy of the diapirs is too weak to allow them to extrude high above the ground surface to form lava domes.

Keywords Kurile islands · Ebeko volcano · Historical eruptions · Mechanism of Vulcanian explosions · Magma diapir · Lava dome

Introduction

The Vulcanian style of volcanic eruptions was first distinguished by Mercalli and Silvestri (1891) who studied the 1888–1890 eruption of Vulcano in the Aeolian Islands. This eruption produced magmas of dominantly intermediate composition, lasted 20 months, and consisted of numerous

separate explosions (Vulcanian explosions) which followed one another with various (although rather regular) intervals lasting from minutes to hours. Vulcanian explosions represented short-lived events lasting only seconds to minutes that produced dark-gray, ash-loaded eruption clouds up to several kilometers high. These explosions also ejected relatively dense ballistic fragments of fresh magma (volcanic bombs), many of which had peculiar “bread crust” surfaces (outer glassy rinds fractured due to syn-eruptive vesiculation and expansion of the inner cores of the bombs).

Modern investigations have shown that Vulcanian-style explosions can have various mechanisms ranging from purely magmatic, where fragmentation of magma is caused by sudden decompression and violent degassing (Diller et al. 2006), to phreatomagmatic where magma explosively interacts with groundwater (Schmincke 1977, Druitt et al. 2002, Nemeth and Kocic 2020). Details on the shifting mechanisms observed at Vulcanian-type eruptions, with recurrent transitions from magmatic to phreatic mechanisms and back to magmatic

Editorial responsibility: N. Métrich; Deputy Executive Editor: J. Tadeucci

✉ A. Belousov
belousov@mail.ru

¹ Institute of Volcanology and Seismology, FED RAS, Petropavlovsk, Russia

² Department of Geoscience, Shimane University, Matsue 690-8504, Japan

³ GFZ German Research Centre for Geosciences, Telegrafenberg, 14473 Potsdam, Germany

episodes, are not well understood and a unifying conceptual model was absent. Ebeko, also Io-Yama or Iwo-Yama (Tanakadate 1936), is a small andesitic volcano complex located in the northern part of Paramushir Island, northern part of the Kurile Island Arc (Fig. 1a, b). Ebeko was named and first described as an active volcano by British geologist and

seismologist John Milne (Gorshkov 1948) who worked in Japan between 1875 and 1895 (Kabrna 2007). The name “Ebeko” means “elevated place” in the language of the indigenous Ainu people. The volcano is one of the most active volcanoes of the Kurile arc (Gorshkov 1970) (Figs. 1c–e and 2). It produced multiple mild explosions in the 20th–21st

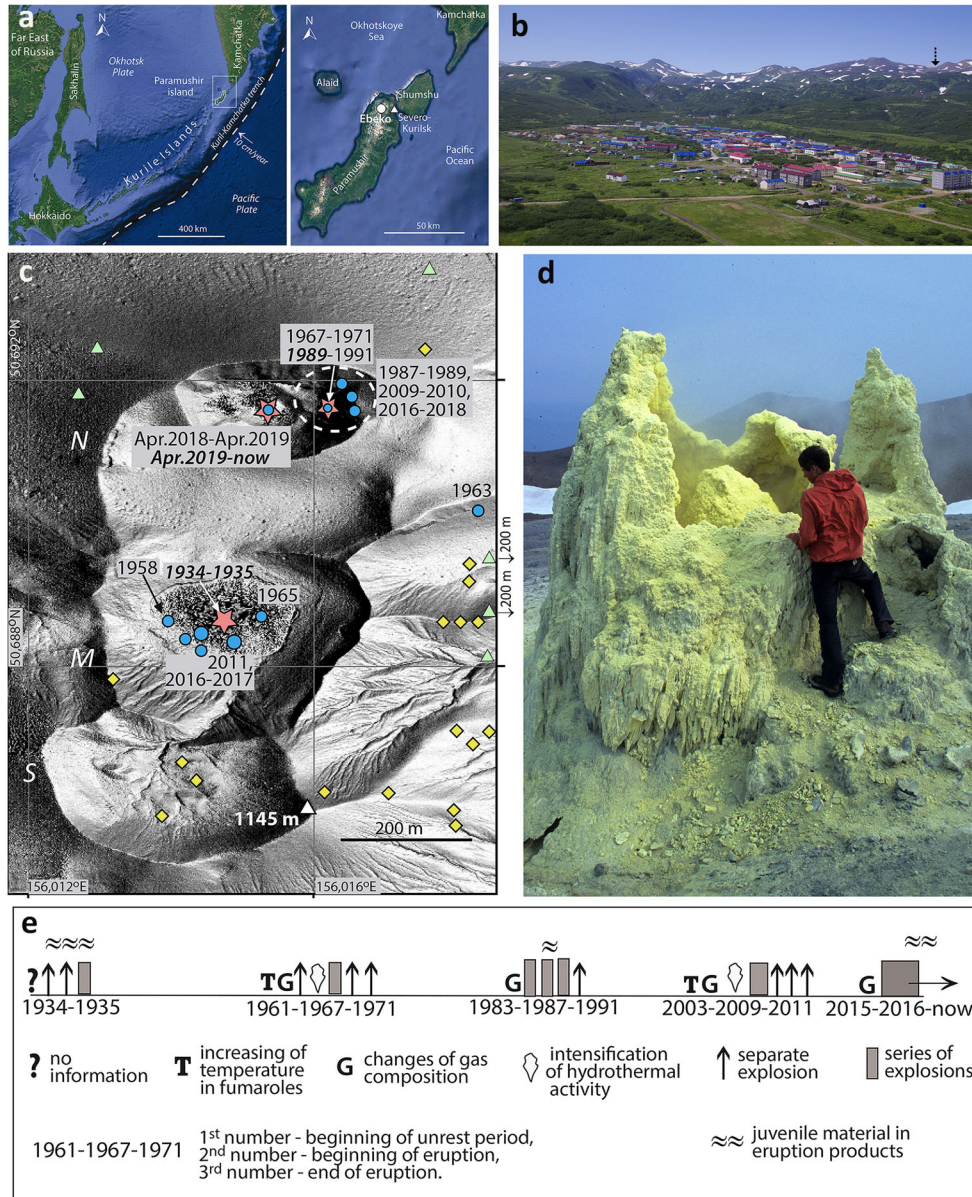


Fig.1 **a** Geographic and tectonic setting of the Kurile Islands and location of Ebeko volcano. **b** Northern part of Vernadsky Ridge. Small monogenetic cones and lava domes of Ebeko volcano are visible along the ridge crest. Position of the new north crater (vent active from 2018 until now) is indicated by arrow. Eastern slope of the ridge is covered by thick block lava flows. Severo-Kurilsk town (in the foreground) is built at the surface of Ebeko's laharic fan. View from the east. Photo courtesy by L. Kotenko. **c** DEM showing the modern morphology of the summit area of Ebeko volcano with three main craters—north (N), middle (M), and south (S), and the highest point of the volcano 1145 m (white triangle). Within the north crater are located new north crater and buried active funnel crater shown by the dashed line. Known dates of eruptions in the

craters are indicated; periods of magmatic activity are highlighted in bold italic. Red stars—magmatic vents, blue dots—non-magmatic vents; the size of the symbols shows relative intensity of eruptions. Vent locations of 1958, 1963, and 1965 after Khramova (1987). Locations of fumaroles and hot springs (yellow diamonds) were identified by the thermal camera of UAS (Walter et al. 2020). Green triangles indicate sampling sites of fresh bread-crust bombs. **d** Sulfur tower in the summit area of Ebeko, 2001. Such sulfur towers periodically appear and disappear in the summit area of Ebeko. Photo by A. Belousov. **e** Timeline of eruptions—schematic representation of documented activity of Ebeko volcano in the 20th–21st centuries. Eruptions commonly occur as a cluster of distinct explosions

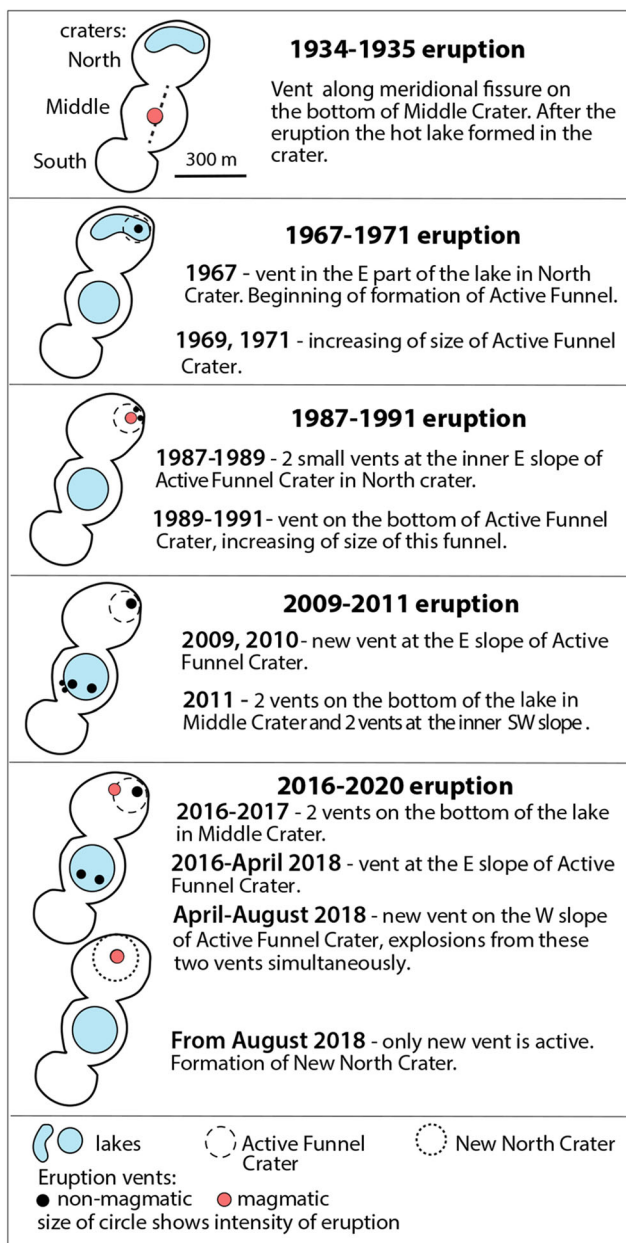


Fig. 2 Schematic representation of documented activity of Ebeko volcano in the 20th–21st centuries on sketches of the summit area with locations of the eruptive vents. Precise locations of the vents are shown on Fig. 1c

centuries (volcano number 290380, Global Volcanism Program). Eruptions of Ebeko are often considered as Vulcanian in a broad sense (according to the classification by Clarke et al. 2015); some of them could be phreatic (hydrothermal); some, phreatomagmatic; and some, magmatic. Details of the eruption dynamics have not been investigated until now.

The main motivation for this study is to review the historical and modern volcanic activities of Ebeko and to understand the character and mechanisms of its eruptions. Since the first detailed studies of the volcano in the late 1950s, most

of the conducted research was focused on water and gas geochemistry. It was expected that changes of the geochemical parameters of the hydrothermal system of the volcano will allow the forecasting of its future eruptions, which pose a threat to the nearby Severo-Kurilsk town (Menyailov et al. 1985). The volcano was also considered as a potential place for the construction of a geothermal power plant (Sugrobov et al., 2005). Apart from the geothermal water and gas geochemistry, the geology and petrology of the volcano remained relatively poorly studied.

In 2019, we conducted fieldwork to investigate the most recent eruptive activity of Ebeko that commenced in 2016. We sampled the erupted pyroclasts, installed seismometers and monitoring cameras, and mapped the terrain using unoccupied aircraft systems (UAS) together with optical and infrared cameras. The seismic and UAS data have shown dimensions and structures of the newly forming crater as well as the distribution and deposition of erupted materials (Walter et al. 2020).

In this paper, we summarize all available observations of the Ebeko eruptions in the 20th–21st centuries, provide descriptions of the 2019 erupted products, and suggest a conceptual model that explains the mechanism of the Ebeko eruptions. In our model, the Vulcanian explosions of Ebeko volcano are caused by shallow intrusions of small diapir-like batches (hereinafter for simplicity referred to as diapirs) of strongly crystallized andesitic magma into water-saturated hydrothermally altered rocks composing the volcano summit.

Geological background

The first geomorphological and geological descriptions of the volcano were published by Tanakadate (1936) and Gorshkov (1958). Ebeko has an elevation of 1145 m asl but lacks a prominent and well-developed volcanic cone (Fig. 1b). Its low-profile, multi-vent edifice is composed of several merged small-volume andesitic lava domes and coulees, intercalated with dense pyroclastic deposits. The edifice is built up on strongly eroded and hydrothermally altered rocks of the SSW–NNE-trending Vernadsky Ridge of Pleistocene age (Fig. 1b).

The broad and rather flat summit area of the volcano is occupied by several overlapping shallow maar-like craters with diameters 200–300 m, surrounded by low rims of dense pyroclasts. The craters were formed in prehistoric times and have different degrees of preservation; many of them are clustered and aligned with the Vernadsky Ridge. The three youngest and best preserved of them (Fig. 1c) are named the north, middle, and south craters. These craters occasionally host shallow temporary lakes originating from snow melting with the addition of fumarolic condensates as currently seen in the middle crater. Based on our drone images and photogrammetric processing, the deepest points within the craters are at very

similar altitudes: at 1085 m in the north crater, at 1124 m in the south crater, and at 1078 m for the lake level of the middle crater (Walter et al. 2020). Since 2018, a small inner crater has developed in the north crater; it was called the new north crater and its floor is located at 1045 m asl (Walter et al. 2020).

The summit area of Ebeko is hydrothermally active with multiple boiling pools, mud pots, and fumaroles (Fig. 1c), some of which periodically build large sulfur towers (Fig. 1d), containing inside pools of bubbling sulfur melt (Kalacheva et al. 2016, Shevko et al. 2018). Native sulfur in the summit area is so abundant that it was mined when the island was under Japanese jurisdiction before 1945 (Tanakadate 1936, Khramova 1987).

Tephrochronological investigations have shown that the modern edifice of Ebeko volcano started to form 2000–3000 years ago (Melekestsev et al. 1994). Past eruptions were moderately explosive with few lava extrusions; the youngest of the lava extrusions occurred approximately 2000 BP.

In 1952, a major megathrust earthquake and a resulting devastating tsunami hit the area, affecting the population on the island (Savarensky et al. 1958). The town Severo-Kurilsk, originally built near the ocean shore at a distance 9 km from the volcano crater, was relocated farther from the ocean towards Ebeko volcano. Now it is located only 7 km away from the active crater. The town is built on top of a gently inclined surface of a volcaniclastic fan, which originates at the mouth of the small river Kuz'minka (Fig. 1b). This river drains the summit area and the eastern slope of Ebeko; its volcaniclastic fan is composed mostly of boulderly deposits of voluminous lahars that occurred at intervals of a few hundred years (Melekestsev et al. 1994). These lahars were probably associated with eruptions of Ebeko that either caused rapid melting of a snowpack, which covers the slopes of the volcano 10 months per year, or breached crater lakes that existed at the volcano's summit, as indicated by deposits of paleolakes exposed in the summit area (Khramova 1987). Some of the lahars were probably not related directly to the volcano's activity, but were caused by strong rains (cyclones) which induced redeposition of the volcaniclastic material as happened most recently in 2017 (Kotenko et al. 2018). An additional hazard is posed by tephra falls from frequent Vulcanian explosions which, together with the accompanying gas emissions, repeatedly caused respiratory problems of the Severo-Kurilsk population (Kotenko et al. 2018).

Methodology

Visual observations/remote sensing

During the fieldwork in July 2019, we acquired field photos and videos, and time-lapse photos, as well as images by a Phantom 4 pro quadcopter UAS, equipped with a 20-MPixel

optical camera and a thermal infrared radiometric camera. The launch site of all drone flights was close to the highest point of Ebeko volcano at 1145 m asl; flight heights were 300 m above this altitude. The aim of the UAS was to provide a general overview and morphologic database. We also placed a geophone seismometer and time-lapse monitoring cameras to record occurrence of explosions. More details on location and type of the instrumentation as well as the processing methods and geophysical records are provided in Walter et al. (2020).

Sampling

Sampling of fresh pyroclasts was conducted between 9 and 15 July 2019; we sampled bombs in freshly formed bomb sags on the western, northern, eastern, and southeastern outer slopes of the active new north crater (Figs. 1c and 3b, c). The bombs were ejected from the crater not long before the sampling, because they were still warm and not covered by fresh ash of the recent ashfalls. Two samples of fresh ash were collected from our clothes in the process of the ash deposition at 15:55 and 16:15 on July 13 at a distance 600 m from the vent.

Grain size analyses

Grain size analyses of 2 ash samples of the ongoing eruption were first performed by standard dry sieving techniques (Walker 1971). Subsequently, the fraction < 0.064 mm (water suspension) was investigated using a Laser Particle Sizer "Fritsch Analysette 22 Compact." Surface morphology of the ash particles was investigated using a Scanning Electron Microscope Tescan Vega 3 in the Institute of Volcanology and Seismology (Petropavlovsk-Kamchatsky, Russia).

Density and vesicularity measurements

Density and vesicularity measurements of the 2019 juvenile material were determined for 4 different bread-crust bombs (2–5 rock fragments of each bomb with the size 2–5 cm). The rock clasts were sprayed with waterproof spray containing silicon oil using the method of Houghton and Wilson (1989) and Hoblitt and Harmon (1993). Density was calculated using the difference between the sample weights in distilled water and air following Archimedes' principle of buoyancy. For the calculation of the vesicularity indexes, the density of non-vesicular low-silica andesite was taken as 2.7 g/cm³ (Mueller et al. 2011).

Petrological analysis

Petrological analysis was performed for 5 bread-crust bombs of the ongoing eruption. Samples were chipped and washed in distilled water and subsequently dried at 120 °C for 12 h. The

Fig. 3 Bread-crust bombs: **a** of the 1934–1935 eruption of Ebeko volcano at the eastern slope of the middle crater, July 2019. **b** Fresh bread-crust bomb, July 2019. **c** Fresh bomb sags at the eastern slope of the new north crater, July 2019. Photos by M. Belousova (**a**) and A. Belousov (**b** and **c**)



samples were then powdered for 90 s, using a tungsten carbide ring mill. Powders were put into a muffle furnace at 900 °C for 3 h to determine loss on ignition (LOI). Fused glass beads were prepared, using an alkali flux consisting of 80% lithium tetraborate and 20% lithium metaborate (Kimura and Yamada 1996). The glass beads were analyzed, using an automatic bead sampler on a Rigaku Co. Ltd. RIX-2000 spectrometer in the Department of Geoscience, Shimane University, Japan. The maximum coefficient of variation is below 1% for major elements and below 10% for trace elements. Standard thin sections were prepared for petrographic description and subsequent analytic. Modal mineral abundance was determined using a semiautomatic point counter with 1000 counts per slide. Mineral and glass compositions were analyzed, using a JEOL 8530F field emission microprobe at Shimane University. Analyses were performed at 15 kV and 20 nA with a focused beam on minerals and a 10- μ m defocused beam on matrix glass. The existence of microlithes prevented a further increase of the beam diameter. In addition, a very short counting time (5 s peak) was used for alkali elements to further prevent sodium loss. Analytical quality was calibrated and monitored using standards provided by the Smithsonian Institute as well as synthetic ones (NMNH164905, NMNH143965, NMNH111312, NMNH115900, NMNH104021 VG2, VG-568, Chromite, Enstatite (synth), Tephroite (synth), Forsterite (synth), NiO (synth), Wollastonite (synth), TiO₂ (synth), NaCl (synth), F-Apatite).

Historical eruptions of Ebeko

Descriptions of the historical eruptions

Here, as well as in Figs. 1c, e and 2 and Table 1, we have summarized the published data of Ebeko activity.

All the observed eruptions of Ebeko in the 20th–21st centuries (1934–1935, 1967–1971, 1987–1991, 2009–2011, and 2016–2020 (ongoing)) were purely explosive and in most cases occurred from new vents that opened at the rather flat summit area of the volcano within the limits of the north or the middle craters (Figs. 1c and 2). The only exception is the 1963 vent that opened at the eastern slope of the volcano (Fig. 1c). Most of the explosive vents were active less than 1 year and produced only one or several short-lived ash outbursts (explosions of 1963, 1965, 1987–1989, and 2009–2011). Such short-lived vents developed small (up to 20–30 m across) and shallow (up to 5–10 m deep) depressions excavated into the superficial preexisting rocks. These vents were surrounded by thin (up to few cm) layers of ejected non-juvenile pyroclasts composed of the fragmented country rocks. These vents quickly disappeared when they ceased to erupt. Such small, monogenetic, transient vents in the Russian volcanological literature commonly are called “explosive funnels,” while larger, polygenetic vents are referred to as “craters” (Menyalov et al. 1990, Kotenko et al. 2007).

In some cases (in 1967–1971, 1989–1991, 2016–2020, and probably 1934–1935), explosive activity of the new vents lasted longer (more than 1 year), producing hundreds to thousands of explosions. In such cases, the small initial vent was gradually enlarged by inward mass wastings that filled/replaced the volume of the country rocks fragmented and ejected by the explosive activity, and with time, the explosive funnels turned into broad (up to 200–300 m wide and 50–70 m deep) maar-like craters deeply excavated into the preexisting rocks. They are surrounded by low-profile mediumly bedded aprons of non-juvenile and, in some cases, both non-juvenile and juvenile dense pyroclasts (bombs and lapilli) up to several meters thick, ejected by the explosions.

Table 1 Summary of the published data about eruptions of Ebeko volcano in the 20th–21st centuries

Eruptions	Period of intensive activity	Period of complete repose	Period of unrest	Juvenile material	Gap between eruptions	References
1934–1935	Oct. 4–17, 1934 Dec. 28, 1934 Jun.–Aug. 1935			Bread-crust bombs		Tanakadate 1936
1967–1971	Febr. 8, 1967–Apr. 1967 Feb. 1969 1971	Sept. 1935–1961	1961–Feb. 1967	No	32 years	Basharina and Khramova 1971; Menyailov et al. 1969, Sidorov 1966
1987–1991	Oct. 14–Dec. 1987 Feb. 2, 1989–Apr. 1990 Jan. 1991 Apr. 4, 1991	1971–1983	1983–Oct. 14, 1987	Juvenile particles in the ash	16 years	Menyailov et al. 1990; Menyailov et al. 1992
2009–2011	Jan. 29–Jun. 18, 2009 Apr. 28, 2010 Jul. 2, 2010 Jul. 16–17, 2011	Apr. 1991–Nov. 2003	Nov. 2003–Jan. 29, 2009	No	18 years	Kotenko et al. 2010, 2012
2016–2020	Oct. 19, 2016–2020 (continues)	2011–2015	2015–Oct. 2016	Bread-crust bombs	5 years	Kotenko et al. 2019, 2020; Walter et al. 2020

Such craters represent relatively long-lasting topographic features. After the eruption cessation due to the continuing inward creep of the wall's rocks, the craters become notably broader and shallower with time, and commonly contain temporary lakes; the water temperature and mineralization/acidity depend on the intensity of the hydrothermal activity in the lake area, which in turn changes with time depending on the volcano activity.

The first historical eruption of the volcano, the details of which are not known, occurred in 1793 (Gorshkov 1958). The next eruption took place in 1859 after 66 years of dormancy. It is known only that this eruption produced extensive clouds of sulfuric gases, which caused respiratory problems on the nearby Shumshu Island at a distance more than 10 km away from Ebeko volcano (Gorshkov 1958).

The 1934–1935 eruption took place after 75 years of dormancy (Tanakadate 1936). It was the strongest eruption of the volcano in the twentieth century that ejected numerous large (up to 4 m across) bread-crust bombs, which can be seen until now (Fig. 3a). It was reported (Tanakadate 1936) that the

eruption took place along a meridional fissure 20 m long, which opened on the bottom of the middle crater (Fig. 2), which was dry at that time. However, it is very likely that the present-day middle crater itself was formed or, at least, strongly modified by the eruption. This eruption was accompanied by extensive outpouring of melted sulfur from fissures that opened at the volcano's slopes. After the eruption ceased, a large hot lake was formed inside the middle crater. Later, with time, the water temperature gradually decreased: the maximal water temperature in 1951 was 90 °C; in 1955, 60 °C; in 1959, 28 °C; and in 1959, 25 °C (Sidorov 1966).

The next 1967–1971 eruption occurred after 32 years of dormancy from the vent formed on the bottom of the north crater that contained a cold shallow lake, which disappeared soon during the eruption (Fig. 2). This vent produced numerous ash outbursts and, after 2 months of activity, by April 1967, reached the size of about 50 m in diameter and 20 m depth (Menyailov et al. 1969). In the steep, nearly vertical inner walls of the vent, the preexisting rocks (hydrothermally altered old pyroclastic deposits and lava flows) were exposed.

Fig. 4 Vulcanian explosions of Ebeko volcano. **a** In 1987, **b–e** in 2018–2019. **a** Sustained ash venting in the active funnel crater in October 1987. **b** Two vents erupt inside the active funnel crater; heights of the ash plumes 50–100 m, April 19, 2018. **c** One of the first explosions 200 m high from the new north crater on August 10, 2018. Middle crater with lake at the foreground. View from the south from the point 1145 m in Fig. 1b. **d** Vulcanian explosion 800 m high at 12:52 p.m. on July 11, 2019. View from Severo-Kurilsk. **e** Vulcanian explosion more than 200 m high at 10:39 a.m. on July 14, 2019. View from the point 1145 m. Photos courtesy of V. Panov (**a**), L. Kotenko (**b**), E. Kotenko (**c**), and A. Belousov (**d** and **e**)



Explosions of this eruption period ejected only old fragmented rocks; no bread-crust bombs were reported.

The large 1967–1971 vent existed until 2018 (Fig. 2). It was mentioned in several papers under the name “active funnel” (Kotenko et al. 2007). Inside this active funnel crater, several small vents of the subsequent eruption periods (1987, 2009–2011, and 2016–2018) were identified. Thus, the active funnel crater can be considered as a long-term, polygenetic crater of Ebeko that displayed sporadic Vulcanian activity in the period 1967–2018.

The next 1987–1991 eruption started after 16 years of dormancy from 2 small vents about 3 m across (Figs. 2 and 4a) formed on the inner eastern slope of the active funnel crater (Menyailov et al. 1990). These vents were intermittently weakly active until February 1989 (Fig. 2). Then, in March 1989, a new vent with diameter of about 20 m was formed on the bottom of the active funnel crater. During the next 2 months, explosive activity from this vent was intensive; heights of the ash clouds reached 5 km. By the end of September 1989, the active funnel crater enlarged up to 140 m across (Menyailov et al. 1992). The intermittent mild explosions with ash clouds up to 2–3 km high continued to occur inside the active funnel crater until the end of the eruption in 1991. No bread-crust bombs were reported throughout the course of this eruption, but juvenile ash particles (glass filaments and bubble shards) were identified in the ash erupted at December 1989 (Menyailov et al. 1992).

The next 2009–2011 eruption commenced after 18 years of dormancy. In 2009–2010, explosions occurred from a new vent formed at the inner eastern slope of the active funnel crater, and in 2011 from four new vents formed in the limits of the middle crater (Fig. 2) (Kotenko et al. 2012). Explosions of this eruption were relatively mild and ejected only old fragmented rocks; no bread-crust bombs were reported.

The last (ongoing) eruption of Ebeko started in October 2016 after 5 years of dormancy (Kotenko et al. 2018). It began from three vents that had been active before (in 2009–2011) (Fig. 2): two vents on the bottom of the middle crater that erupted until May 2017 and the third vent at the eastern rim of the active funnel crater that erupted until August 2018. In April 2018, a new vent appeared at the western rim of the active funnel crater. During the period from April 2018 until August 2018, two vents were simultaneously active inside the active funnel crater (Fig. 4b) (Kotenko et al. 2019). By August 2018, the new vent at the western rim of the active funnel crater further intensified its activity, which was associated with the development of a new crater, while the former active funnel crater was partially buried by the ejected pyroclasts. Eventually, the 2009 vent stopped to erupt, while the new crater evolved and shifted to the west, covering the April 2018 vent (Fig. 2). The April 2018 vent continued to be the only active vent in the north crater for the years thereafter (Fig. 4c). It gradually enlarged and was named “new north crater”

by Walter et al. (2020). Since August 2018, all the explosive activity of Ebeko occurs only inside the new north crater (Figs. 1c and 2).

Starting from July 2018, the explosions from the new north crater became more powerful (Fig. 4d, e), with eruption clouds up to 5 km high (Chibisova and Degterev 2019). In September 23–24 and 29, 2018, heavy ash falls with lapilli up to 3.5 cm in diameter occurred in Severo-Kurilsk. Rumbling sounds, glowing, and lightning were observed above the crater area (Kotenko et al. 2019). The diameter of new north crater in September 2018 was 100 m (Kotenko et al. 2019); in July 2019, 210 m, depth 70 m (Walter et al. 2020).

In the first 2 years of the ongoing eruption, only non-juvenile material was ejected by the explosions, but since April 2019, the ejections of bread-crust bombs are reported (Kotenko et al. 2020). The bombs up to 0.5 m in diameter are ejected to a distance up to 1.5 km from the crater (Fig. 3b, c).

At the time of writing (November 2020), the eruption of Ebeko continues.

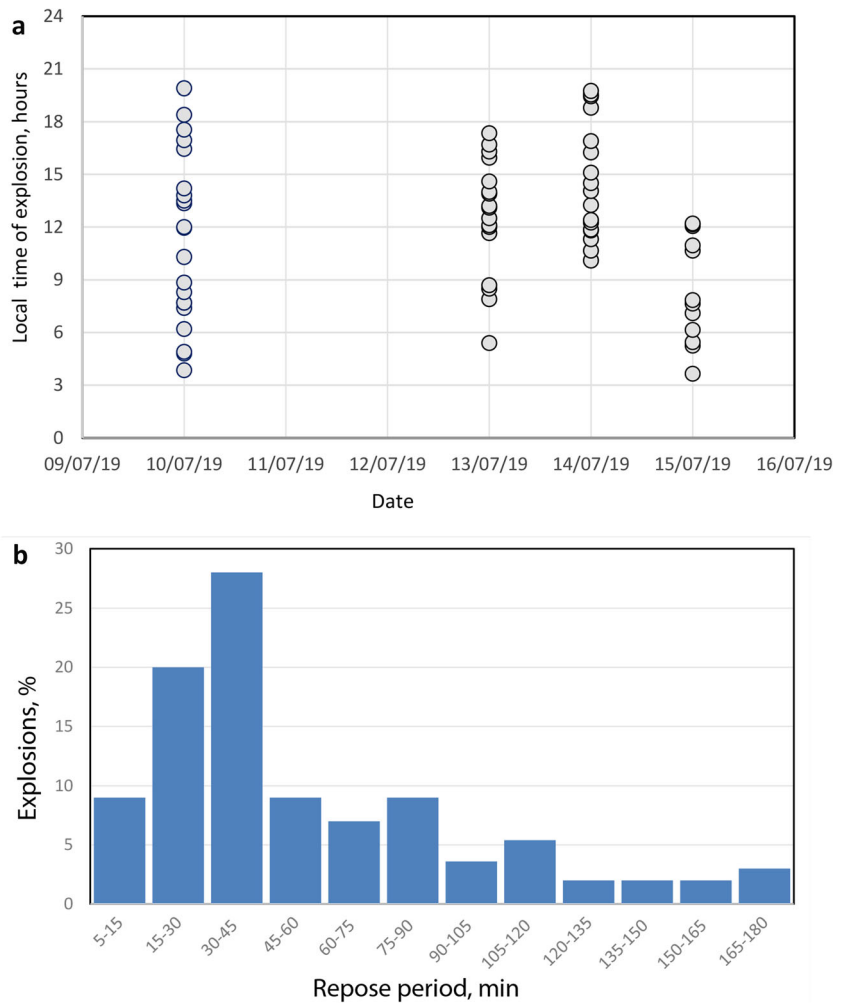
Investigation of the ongoing eruption

During our fieldwork in July 9–15, 2019, the mapping of geomorphological features of the edifice of Ebeko volcano including locations of thermal spots (Fig. 1c) was completed by UAS (Walter et al. 2020).

Monitoring of explosions was achieved by several time-lapse cameras, seismic station, and visual observations from different points around Ebeko including Severo-Kurilsk. During 4 days of good weather (July 10 and 13–15), we have registered the time and the ash plume heights of 61 explosions as well as the durations of the repose intervals between them (Fig. 5a, b). Some of the registered explosions were short-lived, and some had extended duration and multiplet appearance. Commonly, several weak ash outbursts were registered immediately after an initial strong explosion (during a period of 3–5 min) and we count such explosions together as one extended explosion.

The video analysis also allowed estimating the heights of eruption plumes. Relatively strong explosions (with plumes > 1 km high) comprised about 30% of all the observed explosions and medium-sized explosions (with plumes 0.5–1 km high) also about 30%. The most common interval between explosions lasted 30–45 min (28% of all the cases), and the interval more than 2 h between explosions was observed 9 times during the 4 days of observations (Fig. 5b). The average interval of repose for the 61 explosions comprised 56 min. Counting of the explosive events registered by seismometer for the period July 10–14 gave the average interval between explosions as 34 min (Walter et al. 2020). The discrepancy between the results shown here (56 min) and the seismometer (34 min) is probably caused by additional gas/steam

Fig. 5 **a** Time of occurrence of Vulcanian explosions in the new north crater of Ebeko registered by time-lapse cameras and visual observations from different points during the daytime (up to 18 h per day) on July 10, 13, 14, and 15, 2019 (local time = UTC + 11 h). **b** Distribution of durations of repose intervals between the explosions during the 4 days of observations. The most common interval between the explosions lasted 30–45 min



explosions and by ash outbursts not strong enough to be visible on our camera images.

Freshly ejected pyroclasts comprised variably vesicular bread-crust bombs, lapilli, and ash. The ash is well-sorted and coarse-grained and contains few fine particles (15–18% of the fraction < 0.064 mm) (Fig. 6a). Surface morphology of the ash particles (Fig. 6b) is mostly blocky with the vesicularity varying from poor to moderate. Rare vesicles of irregular shapes with dimensions 0.1–0.3 mm are widely scattered over rugged surfaces of ash particles. Surface morphology of the ash indicates that it was produced by fragmentation of poorly to moderately vesiculated, highly crystalline, viscous magma. Low content of fine particles indicates that phreatomagmatic mechanism of fragmentation (due to contact of magma with groundwater) did not play a notable role in the fragmentation process of the ongoing eruption (Wohletz 1983).

Juvenile material of the 4 bread-crust bombs sampled in July 2019 has densities ranging from 1.5 g/cm³ up to 2.6 g/cm³ and the corresponding indexes of vesicularity from 4 to 45%. Together with normal (coherent) magmatic rock, several

of the studied bombs contained juxtaposed coherent and fragmental, pyroclastic-like material (Fig. 7). Particles in the fragmental domains are generally dense, with angular blocky shapes; clast sizes vary between micrometer size (fine ash) up to more than 1 cm (lapilli size). The fragmental domains are fully consolidated and look like either re-amalgamated lapilli tuff (Fig. 7a–e) or sheared and stretched ash bands admixed to the andesite melt (Fig. 7c). Boundaries between the pyroclastic and the magmatic domains are sharp and clearly defined (Fig. 7f). The occurrence of fluidal shapes and the degree of consolidation suggest that the fragmental material has been reheated and partly welded. The pyroclastic domains closely resemble tuffsite described at the 2012 lava dome of Colima volcano, where its formation was associated with violent degassing of magma that fed Vulcanian explosions (Kendrick et al. 2016).

Petrology

Petrological analysis was performed for the 5 bread-crust bombs of the ongoing eruption. The juvenile material is a

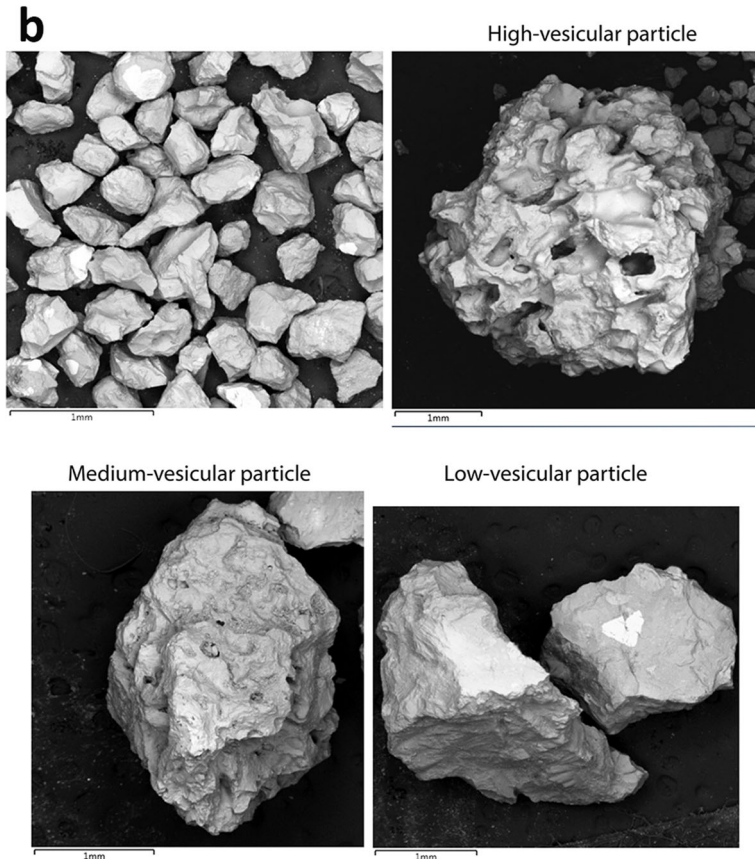
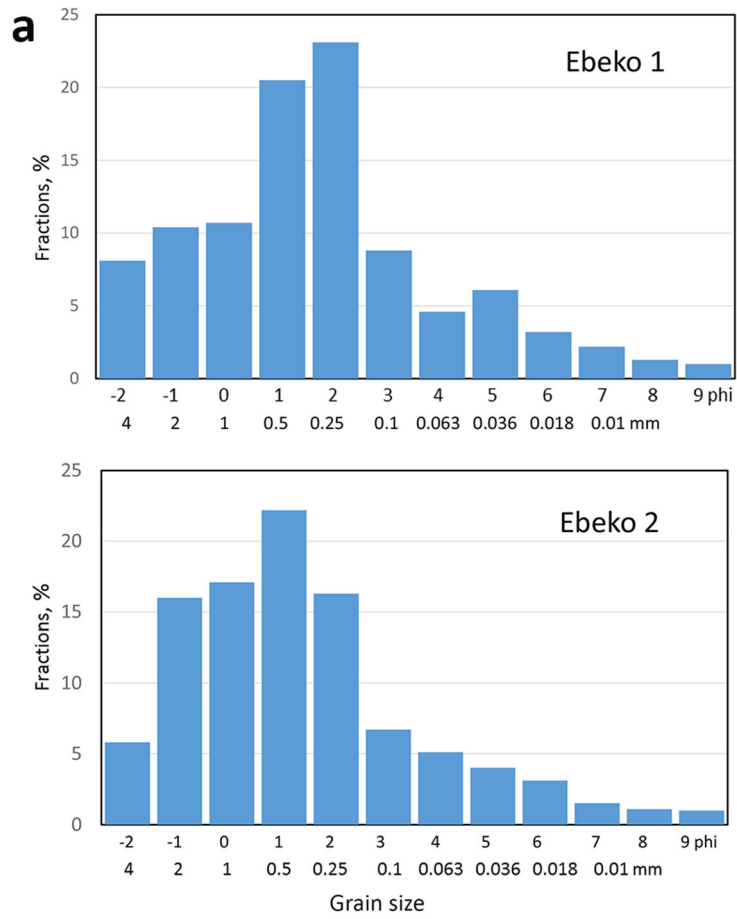


Fig. 6 Characteristics of ash fallout deposits of Vulcanian explosions of Ebeko on July 13, 2019. **a** Grain size distributions of ash samples collected during the ash fallouts at a distance 600 m from the crater, explosion at 15:55 (Ebeko 1) and at 16:15 (Ebeko 2), July 13, 2019. **b** SEM images of surface morphology of the ash particles

highly porphyritic (47–56 vol% crystals) 2-pyroxene andesite containing plagioclase (29–39%), clinopyroxene (7–11%), orthopyroxene (5–8%), oxide (2–3%), and rare olivine (< 1%). The hyalopilitic groundmass has light brownish color and contains microliths of plagioclase and pyroxene.

The whole rock composition of the bomb's material was determined by XRF analysis. Major elements of the bulk rocks and matrix glasses are shown in Table 2, together with published data on the Ebeko suite (Panin et al., 2015). Four samples are low-silica andesites, and one sample is a basaltic andesite (Fig. 8a). The rocks described by Panin et al. (2015) have compositions from basaltic andesite to silica-rich andesite with xenolithic material of basaltic composition.

Altogether, the samples belong to the high-K series (Gill 1981) and plot on the boundary between the tholeiitic and calc-alkaline magmatic series (Miyashiro 1974). The relatively mafic whole rock chemistry is in sharp contrast with the matrix glass composition in all samples, which is exclusively rhyolitic in composition (Fig. 8a). The glass composition

between individual samples (Fig. 8b–e) shows limited variation with slight elevation in potassium content for some samples.

Mineral composition, zoning patterns, and reaction textures

We use high-resolution backscatter images (Fig. 9) as well as stacked histograms (Fig. 10) to illustrate compositional variation and abundance of mineral phases which are subsequently used to develop a petrogenetic model. The potential melt composition (whole rock, glass, and calculated compositions) matches the observed range of phenocrysts chemistry (Fig. 10a). We used mineral melt exchange coefficients and outer error bounds for possible equilibrium of the respective mineral phases from Putirka (2008). All mineral and glass compositions are provided as Electronic Supplementary Table 1.

Olivine occurs in all samples in small quantities (less than 1% modal amount) but still in sufficient quantities to get some representative analytical results. Two textural types are distinguished: the first one occurs as olivine cores mantled by thick orthopyroxene–spinel symplectites, showing characteristic “fingerprint textures” olivine cores (Fig. 9a). These olivines are always compositionally homogenous, and thick mantling

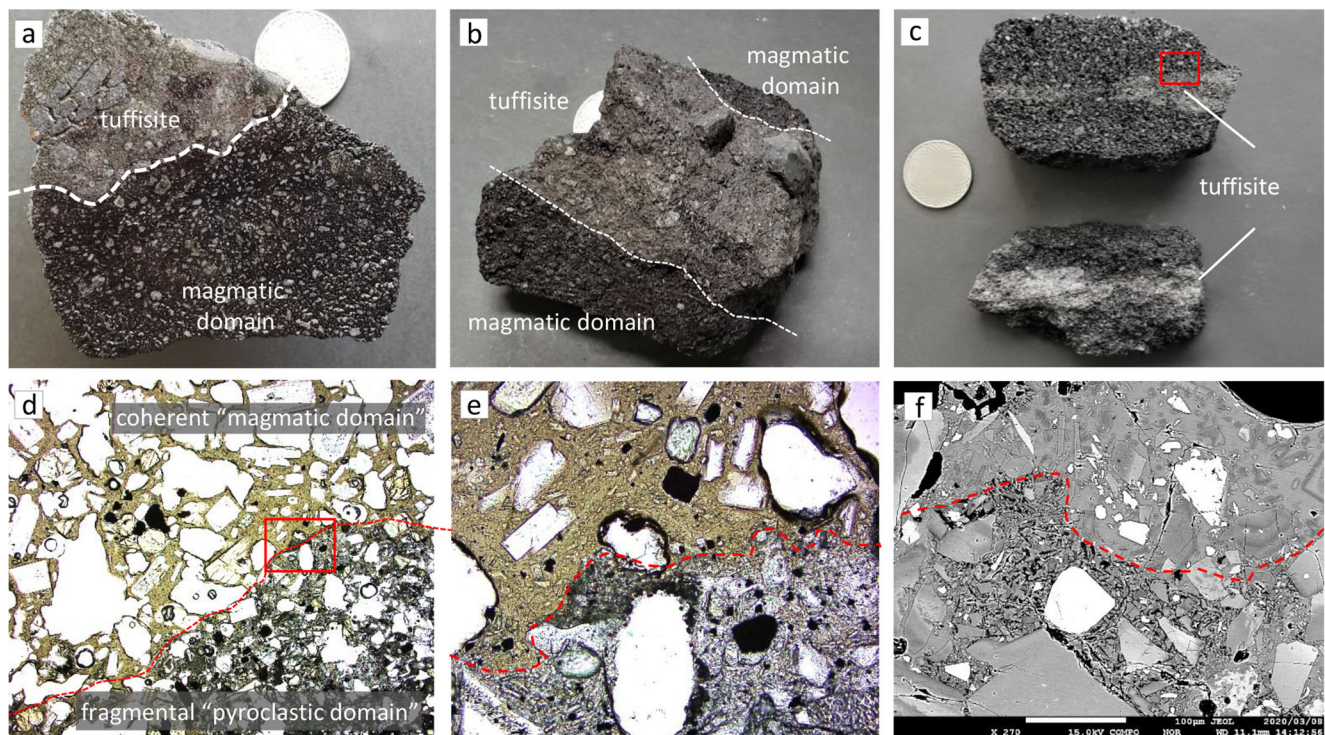


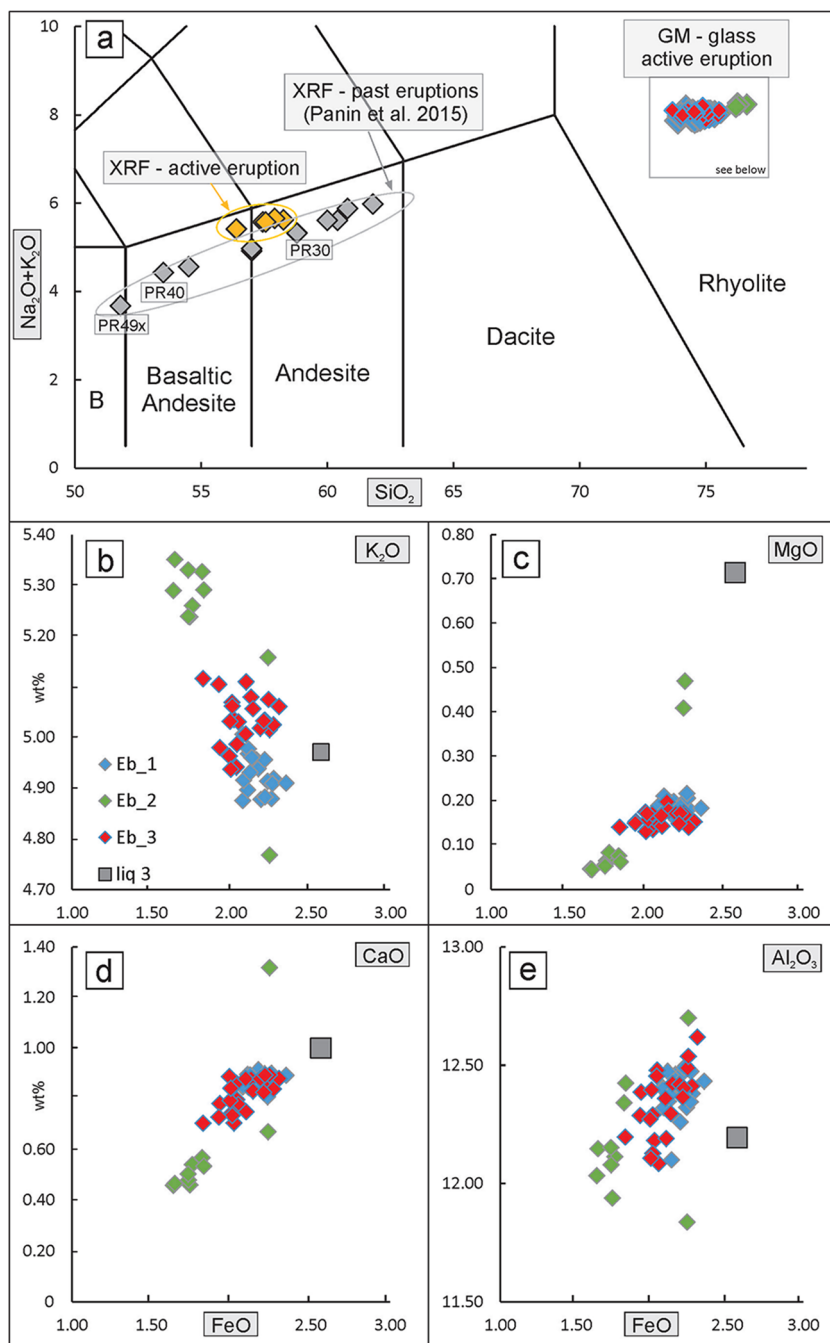
Fig. 7 Macroscopic and microscopic textures from the recent eruption of Ebeko volcano. **a** Fragmental pyroclastic domain (tuffisite) amalgamated to a magmatic domain of highly porphyritic andesite. **b** Broad band of tuffisite welded into a magmatic andesitic domain. **c** Thin band of ash (tuffisite) within a vesicular andesite, showing a shearing texture. **d** Thin

section image (PPL) of a fragmental domain (tuffisite) adjacent to a magmatic domain. **e** Close-up of **d**. **f** Backscatter image showing high-resolution close-up of **e** with a magmatic domain in the upper part and angular clasts in the lower part

Table 2 Element chemistry from this study (whole rock and glass) together with some results from the literature

	Panin et al. 2015										Gm-glass + 2.5% Opx Liq 3					
	This study					This study										
	WR-XRF		WR-XRF			GM-glass-EPMA (n)										
	Pr 40	Pr 30	Eb-4	Eb-1	Eb-5	Eb-3	Eb-2	Eb_1(18)	σ	Eb_2(10)	σ	Eb_3(23)	σ			
SiO ₂	51.8	53.5	58.8	56.39	57.45	57.55	57.91	58.26	SiO ₂	74.65	0.37	75.40	0.87	74.76	0.51	75.24
TiO ₂	0.7	0.78	0.61	0.69	0.65	0.66	0.63	0.64	TiO ₂	0.40	0.02	0.39	0.01	0.41	0.03	0.40
Al ₂ O ₃	15.7	18.1	16.7	17.11	17.24	16.93	17.11	16.86	Al ₂ O ₃	12.38	0.09	12.18	0.24	12.34	0.14	12.19
Fe ₂ O ₃	9.83	9.74	7.54	8.53	8.02	8.07	7.76	7.97	FeO	2.17	0.08	1.84	0.21	2.08	0.12	2.57
MnO	0.17	0.19	0.16	0.18	0.18	0.17	0.17	0.17	MnO	0.06	0.01	0.05	0.02	0.06	0.01	0.08
MgO	8.39	4.3	3.73	3.21	2.95	3.00	2.86	2.89	MgO	0.19	0.01	0.14	0.15	0.16	0.02	0.71
CaO	9.18	9.22	7.04	7.61	7.30	7.11	7.08	6.85	CaO	0.88	0.03	0.60	0.25	0.82	0.06	0.82
Na ₂ O	2.33	2.72	3.11	3.20	3.23	3.19	3.27	3.15	Na ₂ O	3.04	0.05	2.88	0.10	2.99	0.09	2.95
K ₂ O	1.35	1.71	2.21	2.21	2.34	2.39	2.39	2.48	K ₂ O	4.93	0.04	5.23	0.16	5.03	0.05	4.97
P ₂ O ₅	0.14	0.2	0.19	0.18	0.19	0.18	0.19	0.17	P ₂ O ₅	0.05	0.02	0.06	0.03	0.06	0.03	0.06
LOI	0.65	-0.14	0.17	0.00	0.00	0.00	0.00	0.00	Cl	0.20	0.01	0.17	0.02	0.18	0.02	-
Total	100.2	100.2	100.3	99.31	99.54	99.24	99.37	99.43		99.24		99.24		99.24		100
Na ₂ O + K ₂ O	3.7	4.4	5.3	5.4	5.6	5.6	5.7	5.6		8.0		8.1		8.0		7.9
Mg#	62.9	46.7	49.5	42.7	42.2	42.4	42.3	41.8		13.3		11.7		11.8		33.2
Calculated melt viscosity, assuming variable P-T-H ₂ O-phenocryst content	Viscosity calculation - based on whole rock composition													Viscosity calculation - based on groundmass glass composition		
T _{liquid}	Pr 49x	Pr 40	Pr 30	Eb-4	Eb-1	Eb-5	Eb-3	Eb-2		Eb_1	Eb_2	Eb_3		Eb_3		
Liquid viscosity log η [Pa*s], (Giordano et al. 2008)	1200.0	1100.0	1100.0	1100.0	1100.0	1100.0	1100.0	1100.0	1100.0	1000.0	1000.0	1000.0	1000.0	1000.0	1000.0	1000.0
wt% H ₂ O	1.9	3.3	4.1	3.9	4.1	4.1	4.2	4.2		7.6	7.7	7.6		7.6		7.6
Liquid viscosity log η [Pa*s], (Giordano et al. 2008)	3.0	3.0	3.0	2.0	2.0	2.0	2.0	2.0		2.0	1.0	0.0		0.0		0.0
Xtal proportion	0.8	1.6	2.1	2.2	2.4	2.4	2.4	2.4		4.9	5.8	7.6		7.6		7.6
Liquid + xtal viscosity log η [Pa*s], (LeLosq et al. 2015)	0.0	0.0	0.0	0.0	0.0	0.0	0.05	0.10		0.1	0.2	0.3		0.3		0.3
Interpretation	0.8	1.6	2.1	2.2	2.4	2.4	2.5	2.6		5.0	6.2	8.3		8.3		8.3
	LCHZ: effective liquid fractionation frequently produces batches of high T, aphyric melts with low viscosity Lower-middle crust: limited crystallization/pressure reduction/-cooling has only mild effect on melt viscosity Upper crust: extensive crystallization drives liquid evolution to rhyolitic composition. In addition, volatile loss and an increasing amount of phenocrysts increase viscosity several orders of magnitude															

Fig. 8 **a** TAS diagram, for products of the ongoing eruption as well as a broader range of erupted products from Ebeko volcano from Panin et al. (2015). **b** Harker diagram, showing major element variation in groundmass glass composition. The sample denoted “b-e Liq3” is a calculated potential liquid to match orthopyroxene chemistry (see details in text)



orthopyroxene prevents further re-equilibration with any surrounding liquid phase. The second type (Fig. 9b) is also always mantled by orthopyroxene, but shows gradual diffusive iron enrichment in the outer zones. Symplectitic reaction textures are not present in this type. The most mafic olivines (Fo₈₀) are not in equilibrium with the whole rock composition. Diffusive iron enrichment and subsequent reaction with a silica saturated melt show that olivine is a relict phase in all samples. Panin et al. (2015) describe rare olivine xenocrysts from Ebeko volcano with high Mg# (Fo₈₀-Fo₉₁) and some

even with elevated Ni contents (~up to 0.3 wt%) suggesting their origin in the sub-arc mantle.

The most mafic orthopyroxenes are associated with olivine reaction textures (Fig. 9a, b). These crystals are usually more magnesium rich at the contact with the olivine and, like the latter, often show diffusive iron enrichment in their outer rims. Composite orthopyroxene and clinopyroxene occur together in all samples. They show a very large compositional range and complex disequilibrium textures (Fig. 9c-f). A distinct population of pyroxenes shows orthopyroxene cores

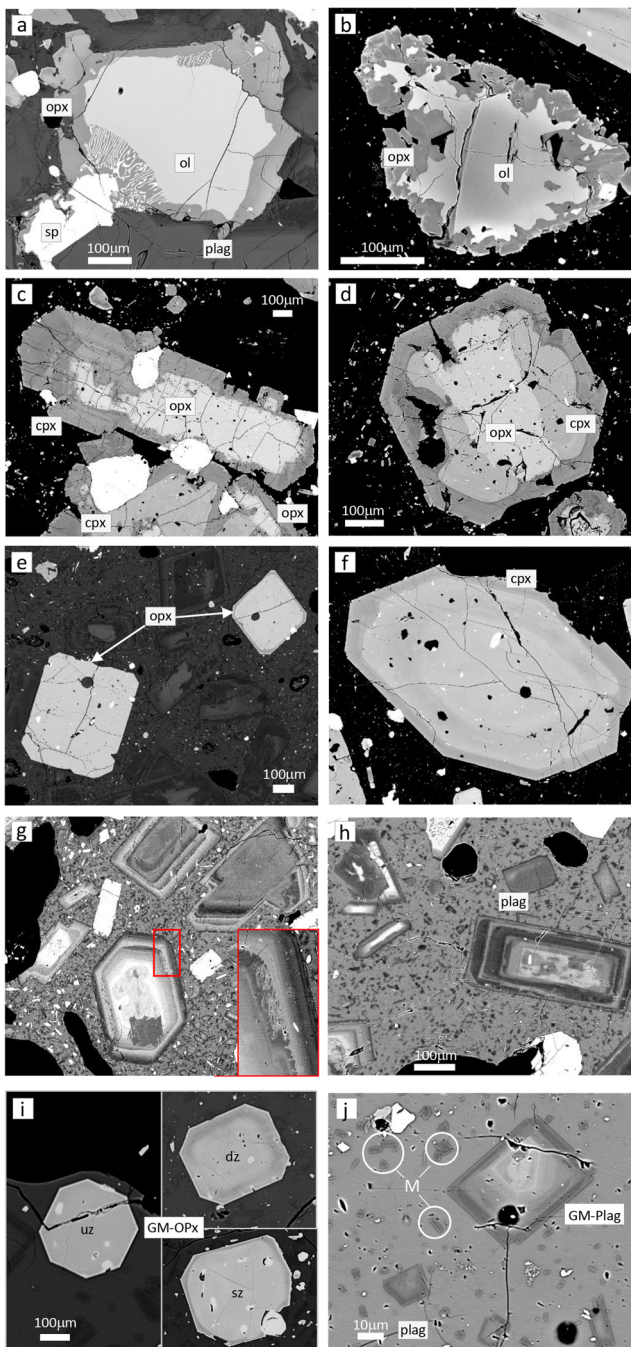


Fig. 9 Textural characterization of pyrogenic minerals. **a, b** Disequilibrium textures—olivine: small amounts (< 1%) of olivine occur in all samples. They are found either as homogeneous cores of symplectite aggregates associated with high An# plagioclase (**a**) or as relict cores mantled by thick Mg-rich orthopyroxene rims (**b**). In the latter case, olivine often shows diffusive gradients to more Fe-rich outer zones (**b**). **c, d** Disequilibrium textures—pyroxene: a large number of orthopyroxene and clinopyroxene phenocrysts show complex disequilibrium features. A particular common texture is the breakdown/overgrowth of orthopyroxene by one (**c**) or several distinct rims of clinopyroxene (**d**), presumably during events of mafic recharge. **e, f** Phenocrysts—pyroxene: orthopyroxene and clinopyroxene also occur as more simple phenocrysts which can show either no zonation or reverse zonation (**e**). Reverse zonation can be either diffuse (**f**—inner part of the crystal) or sharp (**e**—right crystal, **f**—outer rim). Normal zonation in both pyroxene varieties is very rare. **g, h** Phenocrysts—plagioclase: Plagioclase is the dominant phenocryst phase in all samples, ubiquitously showing complex oscillatory zoning patterns, often with cores showing resorption symplectite textures (**g, h**). A snapshot of an incipient resorption reaction is preserved in the rim of a phenocryst in (**g**). In smaller phenocrysts, normal zoning prevails. **i, j** Groundmass microphenocrysts (< 100 μm) occur in large numbers, evenly distributed within the groundmass. GM-OPx (**i**) can either be unzoned (uz), diffusely reverse zoned (dz) or sharply reverse zoned (sz). Plagioclase microphenocrysts are generally normal zoned (**j**). Microlithes(M): Na-rich plagioclase microlithes (< 10 μm) are also ubiquitous in all samples

the groundmass. They are either unzoned, diffusely reverse zoned, or sharply reverse zoned (Fig. 9i). The majority of these crystals have low magnesium numbers, but some show high magnesium numbers, thus spanning the entire spectrum of orthopyroxene composition. The majority of orthopyroxene crystals (the large mode around Mg# 64–65) has no observed equilibrium melt composition to match with (Fig. 10). Hypothetical equilibrium can be achieved by either incrementally adding ~2.5 wt% orthopyroxene back to the groundmass glass composition, or by removing ~2.5 wt% from the most silica-rich whole rock composition (sample PR32 from Panin et al. 2015). Clinopyroxene does not occur as a ubiquitous groundmass phase.

Plagioclase shows a wide variety of textures (Fig. 9g–h, j) and also spans a large compositional range (Fig. 10). The most anorthite-rich compositions are found in association with the olivine symplectites, where olivine and orthopyroxene are occasionally intergrown with plagioclase (Fig. 9a). The most calcium-rich compositions (An_{91} – An_{95}) are found adjacent to the mafic mineral cores, and outer rims are generally more sodic in composition. Like the olivine symplectites, these associated plagioclase crystals are considered a relict phase. The majority of plagioclase feldspars show compositions between An_{45} and An_{75} (Fig. 10b). This compositional variation is often encompassed within a single crystal (Fig. 9g, h), with some crystals showing one or several symplectitic zones of resorption (Nakamura and Shimakita 1998) and subsequent overgrowth. In addition to the complex oscillatory zoned phenocryst population, we distinguish again groundmass

overgrown by one or even several magnesium-rich clinopyroxene rims (Fig. 9c, d). Magnesium number distribution (Fig. 10a) clearly shows that in these aggregates, orthopyroxene and clinopyroxene are related to distinct melts respectively. In addition, orthopyroxene and clinopyroxene occur as large (up to 2 mm) phenocrysts which can be completely homogenous, simple or multiple normal or reversely zoned (Fig. 9e, f). A further group of orthopyroxene is distinguished here as groundmass microphenocrysts (GM-OPx < 100 μm). These crystals are generally euhedral and occur homogeneously dispersed in large number throughout

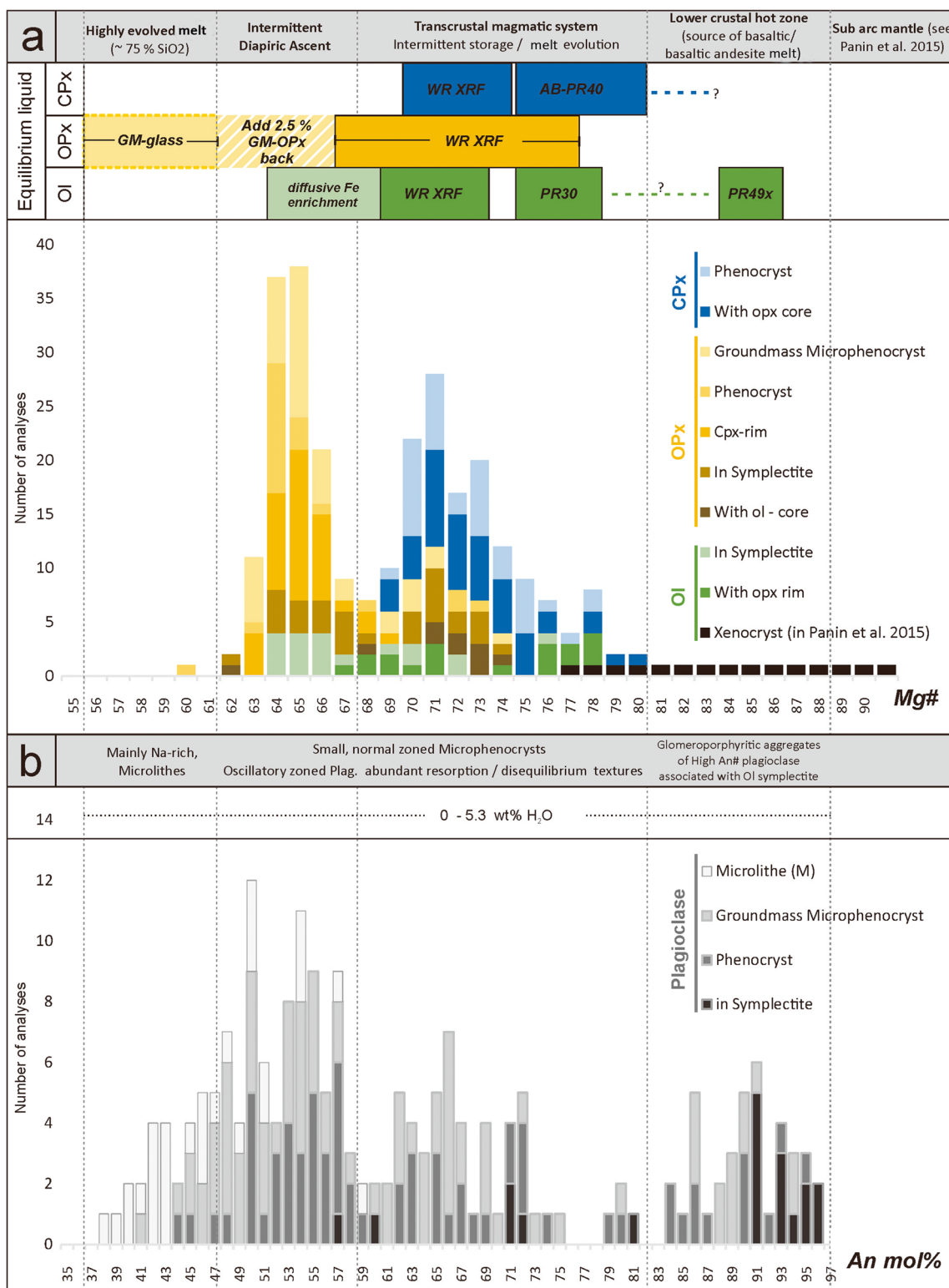


Fig. 10 Compositional variation of phenocrysts for mafic minerals (a) and plagioclase (b). The colored bars at the top match potential melt composition (whole rock, glass, and calculated compositions) to the observed range of phenocryst chemistry

microphenocrysts (GM-Plag < 100 mm) and plagioclase microlithes (M). Groundmass microphenocrysts are mostly normal zoned (Fig. 9j) and also span a very large

compositional range (~An₉₀–An₄₅). Plagioclase microliths (M) are Na rich and always normal zoned or homogenous with the majority showing An# of less than 50 down to An₃₈.

Discussion

Erupted magma and its storage conditions

Several thermobarometers are applicable to the phase assemblage in our samples. The challenge is to infer suitable equilibrium melt compositions to perform the task. The following calculations were made using the models for the melt: olivine-melt, orthopyroxene-melt (Putirka 2008), clinopyroxene-melt (Neave and Putirka 2017), and plagioclase-melt hygrometer (Lange et al. 2009). Two-pyroxene thermometry was not used, since many samples suggest orthopyroxene and clinopyroxene disequilibrium between two or several melts (Fig. 9d). The least evolved melt composition known from Ebeko volcano was presented in Panin et al. (2015) who also mentioned the presence of high-Mg# olivine with elevated Ni contents. Unfortunately, this work does not describe these rocks in detail, since the main focus of the paper is not igneous petrology. Applying a melt thermometer to the basalt composition (Eq. 14 in Putirka 2008) yields a temperature of 1227 °C. Adding water will slightly lower the melt temperature (e.g., 1194 °C at 3 wt% H₂O). No detailed olivine compositions are reported for this basalt, beyond the fact that they range in composition from Fo₇₇ to Fo₉₁. Olivines found in our samples are iron richer, and we infer that they have been in equilibrium with one of the mafic andesites or basaltic andesites (e.g., PR30). Melt thermometry for PR30 yields 1055 °C (1088 °C anhydrous), and pairing equilibrium olivines with

sample PR30 (Eq. 22) yields temperatures of 1038 °C (1087 °C anhydrous).

The range of observed orthopyroxene composition is not in equilibrium with only one single melt, but instead can be matched up successively with different melts, each for a limited range of compositions. In addition, the largest population of orthopyroxene is not in equilibrium with any observed melt. However, a hypothetical equilibrium melt can be obtained by adding orthopyroxene to the groundmass composition (hatched bar in the top section of Fig. 10) or by subtracting it from a silicic whole rock composition (Danyushevsky et al. 2000). Orthopyroxene associated with olivine cores and olivine symplectites yield distinct P - T values when combined with mafic melt compositions (Fig. 11). The P - T range of orthopyroxene phenocrysts varies widely and is strongly dependent on the choice of melt and water content, but generally falls between 950 and 1050 °C and 0–400 MPa. Clinopyroxene P - T crystallization conditions crudely match those of orthopyroxene, generally showing slightly higher temperatures. Results from plagioclase hygrometry (Lange et al. 2009) were highly variable, given the degrees of freedom, when considering the available range of phenocryst compositions, melt compositions, and temperatures. If considering the high An# plagioclase associated with olivine symplectites and the respective olivine melt temperatures, plagioclase hygrometry yields maximum water content in the melt as 3%. Applying the entire observed range of plagioclase compositions with possible melt compositions (approximately

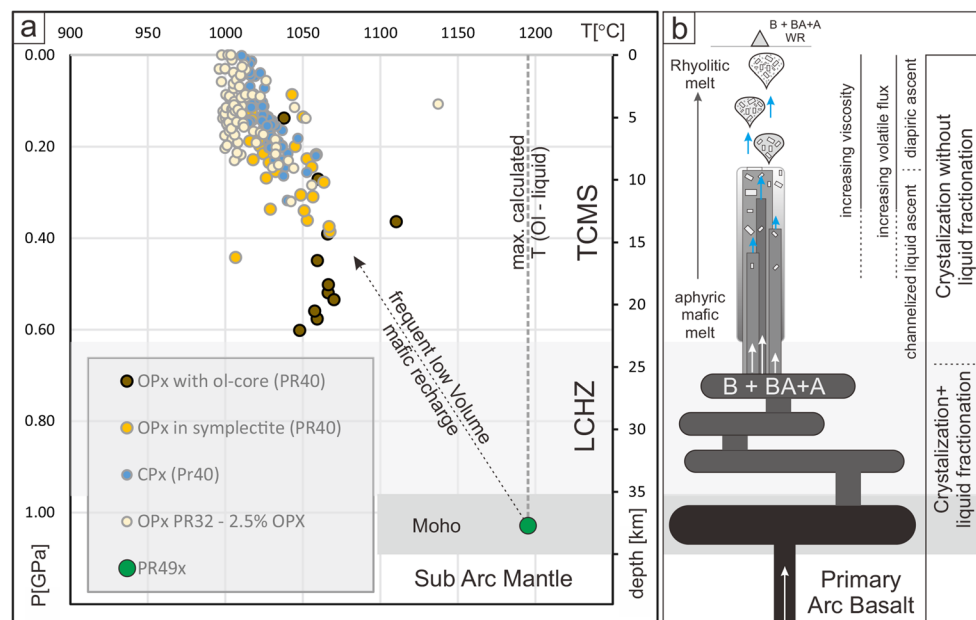


Fig. 11 Calculated P - T range for the observed phenocrysts (a) and petrogenetic scheme (b). Primary arc magma undergoes fractional crystallization in a lower crystal hot zone. Small batches of fractionated melt (basaltic-andesitic) will undergo additional extensive crystallization without melt fractionation. In such a configuration of the transcrustal magmatic system (TCMZ), small aphyric magma batches of relatively

low viscosity will detach from the low crust hot zone (LCHZ) and subsequently undergo significant crystallization (\pm mixing/ stagnation/ differentiation) upon ascent through the crust. They are reaching the ground surface as diapirs of highly viscous, crystal-rich rhyolitic melt of intermediate whole rock (WR) composition

following the compositional range that matches plagioclase and melt in Fig. 10) yields contents of water in the melt between 5.3 and 0%. In addition, textural considerations suggest that completely degassed melt occurs together with volatile rich melt in the very shallow magmatic system similar to those described in Lautze et al. (2007) with juxtaposed high-density and low-density domains.

The following stages are important, when considering the melt evolution at Ebeko volcano (Fig. 11). Primary arc magma will rise and stall at the Moho. Subsequent melt evolution is presumed to take place in a lower crustal hot zone (LCHZ) as described by Annen et al. (2006). Prolonged crystallization and storage times will allow crystallization and melt fractionation. The forthcoming melts will be of basaltic, basaltic andesite, and low-silica andesitic composition and assumed to be largely aphyric. Small batches of these melts will be frequently injected into a transcrustal magmatic system (TCMS). Here, further extensive crystallization will take place without melt fractionation. As a consequence, erupted melts are of rhyolitic composition while maintaining their mafic–intermediate whole rock chemistry (Auer et al. 2013, 2016). In addition, frequent injection of small batches of new melt will also provide a sustained source of volatiles (but not an extensive local pressurization of the system). Sustained melt and volatile flux in the middle and upper crust will then drive regular ascent of small magma diapirs from the upper part of the system. The fact that material from deep within the system frequently reaches the surface shows that currently, no long-living extensive crustal magma storage zone exists. Such arrival of primitive magma is common, not only for simple island arcs but also through thick continental crust (Ozerov et al. 1997; Winslow et al. 2020). One of the key results of these petrogenetic processes is the fact that, despite their relatively mafic whole rock composition, magmas of Ebeko possess high viscosity, due to their evolved melt composition and very high crystallinity.

Evolution of melt viscosity

In the following section, we perform theoretical calculations of the melt viscosity (Table 2). The results of these calculations will be used to elaborate the proposed functional model of Ebeko volcano (see discussion below).

The viscosity values of magma, which is a three-phase mixture of melt containing dissolved water with crystals and gas bubbles, can be calculated based on chemical composition (Giordano et al. 2008) and volume fraction of crystals (Le Losq et al. 2015; Métrich et al. 2016). The amount of dissolved water is accounted in the Giordano et al. (2008) model. We assume different volatile content as well as different amounts of crystal content for the entire range of compositions. The key question is which composition is the best representative of the melt phase—the whole rock or the matrix

glass? Strictly speaking, only matrix glass is the true representative of the melt phase during the eruption, while the whole rock composition represents the mixture of phenocrysts and the glass and therefore is not a true representative of the melt phase. Models of lower crustal hot zones (Annen et al. 2006) have shown that fractional crystallization works more efficiently in the lower crust than in the upper crust. Therefore, mainly aphyric melts can fractionate from the LCHZ and ascend into the upper crust. Assuming that products of subsequent crystallization largely remain in the melt (Fig. 11b), the calculated whole rock viscosities will be representative as true melt viscosities for the lower and middle crust (containing substantial amounts of dissolved H₂O but negligible amounts of crystals). In other words, we assume that at Ebeko the bulk input composition from the LCHZ into the upper crust is approximately equal to the bulk output composition during the eruption. The only difference is that the melt in the lower crust is mafic and aphyric, whereas it is highly crystallized and rhyolitic when it reaches the surface. In such a configuration of the transcrustal magmatic system, small aphyric magma batches of relatively low viscosity will detach from the LCHZ and subsequently undergo significant crystallization (\pm mixing/stagnation/differentiation) upon ascent through the crust. They are reaching the ground surface as diapirs of highly viscous, crystal-rich rhyolitic melt of intermediate whole rock composition.

Frequency and character of Ebeko eruptions

The historical activity of Ebeko volcano is difficult to subdivide into discrete eruptions because it consisted of separate short-lived explosions divided by highly variable hiatus intervals, lasting from seconds to years. Obviously, it is not practical to count each explosive outburst as a separate eruption because they were too numerous to count, and not all of them were registered. Here, we define eruptions as periods of relatively high activity with rather frequent explosions separated by inter-eruptive periods with no or rare explosions. During the last 100 years, for which at least some observational data of the Ebeko activity exist, 5 eruptions (or periods of high explosive activity) of the volcano can be tentatively distinguished: 1934–1935, 1967–1971, 1987–1991, 2009–2011, and 2016–2020 (ongoing) (Table 1, Fig. 1e). The first four of them consisted of separate explosions or series of frequent explosions divided by hiatus intervals lasting from 2 months up to 2 years. During the last eruption, starting from 2016, the hiatus intervals probably did not exceed 1 day.

Inter-eruptive periods

Inter-eruptive periods of Ebeko can be subdivided into the post-eruption repose periods, when parameters of the surface manifestations of the hydrothermal system of the volcano

gradually return to the background level, and the pre-eruption unrest periods, when parameters of the surface manifestations of the hydrothermal system of the volcano gradually start to change (intensify) before the forthcoming eruption (Menyailov et al. 1985).

Periods of pre-eruption unrest for the four relatively well-observed eruptions of Ebeko have been 1–6 years long (Fig. 1e, Table 1), when the temperature of fumaroles sometimes increased up to 500 °C (Kalacheva et al. 2016). During some of the observed periods of unrest, episodic steam/hydrothermal explosions and voluminous outpourings of molten native sulfur were reported in the summit area of the volcano (Fig. 1c). Active sulfur flow observed in 1963 was 0.5 m wide and 5–10 cm thick (Sidorov 1966). Similar flow was observed in 1965 (Skripko et al. 1966). Obviously, such large volumes of sulfur could not be deposited from fumarolic gases during the corresponding period of unrest. Such large volumes of sulfur melt probably originate from ancient sulfur-bearing deposits, possibly the deposits of ancient crater lakes that are buried in the summit area of the volcano (Khramova 1987). The ascending magma heats up the sulfur-bearing country rocks, which causes melting and mobilization of the sulfur (Vlasov 1958). Further increase of the temperature leads to burning and sublimation of the buried pre-accumulated sulfur, that in turn produces extensive clouds of suffocating sulfuric gases reported during some of the pre-eruption periods, e.g., in September 2005–May 2006 (Kotenko et al. 2007).

Vulcanian eruptions of Ebeko

Analysis of the published data as well as our observations in 2019 show that the character of Ebeko eruptions in 20th–21st centuries was visually rather uniform. The volcanic activity was purely explosive and consisted of series of frequent (with intervals minutes-hours) short-lived moderately concentrated (gray-dark gray) ash outbursts with ash clouds rising commonly up to 1 km high, and in rare cases up to 5 km high. Some of the outbursts were more extended in time (represented sustained ash venting that lasted from minutes to several hours). The dynamics and visual appearance of the ash outbursts at Ebeko in general fit the classic visual appearance of Vulcanian-style explosions (Mercalli and Silvestri 1891), as was first mentioned by Tanakadate (1936). Pyroclastic material ejected by the visually similar Vulcanian outbursts during the considered period of Ebeko activity, however, was not uniform. Some of the outbursts undoubtedly ejected juvenile material (in the form of bread-crust bombs). Such outbursts prevailed during the second half of the ongoing eruption (from 2019 until now) and probably were common during the 1934–1935 eruption. Less confident is the presence of juvenile material during the final part of the 1987–1991 eruption. The other eruptions of Ebeko (1967–1971 and 2009–2011) consisted of Vulcanian outbursts that ejected only non-

juvenile material (fragmented country rocks represented by hydrothermally altered old lavas and pyroclasts). Thus, during about half of the observed eruptions of Ebeko, the juvenile material was erupted, which means that andesitic magma reached and breached the ground surface. During the other half of the observed eruptions, no juvenile material was erupted. However, the observed non-magmatic explosive activity and the perturbations of the hydrothermal activity during the preceding periods of unrest allow us to suggest that fresh magma, although was not erupted, probably did ascend to the shallow subsurface level.

Mechanisms of Vulcanian explosions were debated for a long time (Morrisey and Mastin 2000). The main question is as follows: Are they purely magmatic, phreatomagmatic or phreatic? Since the work of Melekestsev et al. (1994), who studied prehistoric ashes of Ebeko buried in soil, all eruptions of this volcano have been commonly described as phreatic and/or phreatomagmatic. Such interpretation was based on old outdated views that juvenile material in volcanic ashes of magmatic eruptions must be represented by glass particles having fluidal morphologies whereas glass particles with blocky morphologies as well as highly crystalline particles are the products of phreatic eruptions. Nowadays, however, it has long been established (Heiken and Wohletz 1985) that morphologies of juvenile particles of magmatic eruptions strongly depend on the viscosity and crystallinity of the erupting magma, and eruptions of andesitic magmas, like those erupted by Ebeko, commonly produce blocky, highly crystalline particles (Clarke et al. 2015).

Our data on the dynamics and the eruption products of the recent eruption of Ebeko clearly demonstrate that this eruption, as well as probably half of the previous historical eruptions of this volcano, has magmatic mechanisms (associated with violent unsteady degassing of magma) and the other half, phreatomagmatic and phreatic/hydrothermal mechanisms (associated with violent boiling of shallow groundwater and/or hydrothermal fluids). Because in most cases the ejected pyroclastic material was not thoroughly studied, it is no longer possible to determine which of the past explosions of Ebeko were of phreatomagmatic origin.

The activity of Ebeko was analyzed during the considered period. A summary of its peculiarities is as follows:

1. Very low precursory seismicity. However, this can be, at least in part, just an artifact. The only seismic station at Ebeko is located in the Severo-Kuril'sk with a high level of ambient anthropogenic noise that does not allow detecting the weak volcanic earthquakes. Some of Ebeko's eruptions (e.g., 1934–1935) were preceded and accompanied by felt earthquakes (Tanakadate 1936). The high rate of recurrence of these earthquakes allows suggesting that at least some of them might be of volcanic origin (not tectonic).

2. Long durations (extended style) of the eruptions and long periods of the pre-eruption unrest. This is probably connected with slow ascent/discharge rate of magma due to its high viscosity.
3. Shifting mechanisms of the eruptions with recurrent transitions from magmatic to phreatic mechanisms and back to magmatic episodes.
4. Overall low explosivity of the eruptions, including the absence of plinian eruptions in the eruption history.
5. Few lava domes/flows in the eruptive history.
6. Lack of main edifice and migrations of the craters, possibly associated with an unstable feeding system.
7. Strong hydrothermal activity in the summit area.
8. Large volumes of native sulfur as well as sulfuric gases emitted during periods of the pre-eruption unrest

To explain the above peculiarities of Ebeko's activity and its geological structure, we suggest a functional model of the volcano and the new "fishing float mechanism" of Vulcanian eruptions.

Functional model of Ebeko volcano

Magma feeding system: slowly ascending chains of diapirs

On Earth, there are many andesitic volcanoes, which demonstrate nearly continuous long-term Vulcanian eruptions of mild intensity that occur from vents with rather stable position at the ground surface. Such eruptions gradually build large symmetric volcanic cones composed of lava flows and pyroclasts with a vent/crater having fixed/constant position on the cone's summit. The examples include volcanoes Karymsky (Kamchatka, Russia), Semeru (Java, Indonesia), Tungurahua (Equador), Colima and Popocatepetl (Mexico). It is plausible to suggest that the feeding system of such volcanoes consists of a simple, vertical pipe-like conduit that connects the magma source and the vent. The conduit is continuously active (filled with the ascending magma melt), and magma does not solidify.

Such a model of a feeding system obviously cannot be applied to Ebeko where the eruption vent has no fixed position. As a result Ebeko has no well-defined cone: its several small monogenetic edifices and craters are scattered along the faulted ridge crest.

Surface migrations of vents/craters as well as long repose periods of Ebeko allow suggesting that magma of this volcano probably ascends to the surface, not through a stable conduit and not through the newly formed fissures/dikes, because few eruption fissures were reported at the volcano and magma of Ebeko is obviously too viscous (Table 2) to be squeezed through the narrow fissures to form dikes. Nevertheless, it may be assumed that ascent pathways are controlled by the preferred alignment along the Vernadsky ridge and at depth

magma possibly forms elongated blob-like bodies or even thick dikes. Also reversely: as Ebeko has no defined cone, it cannot establish a fixed magma pathway (Maccaferri et al. 2019).

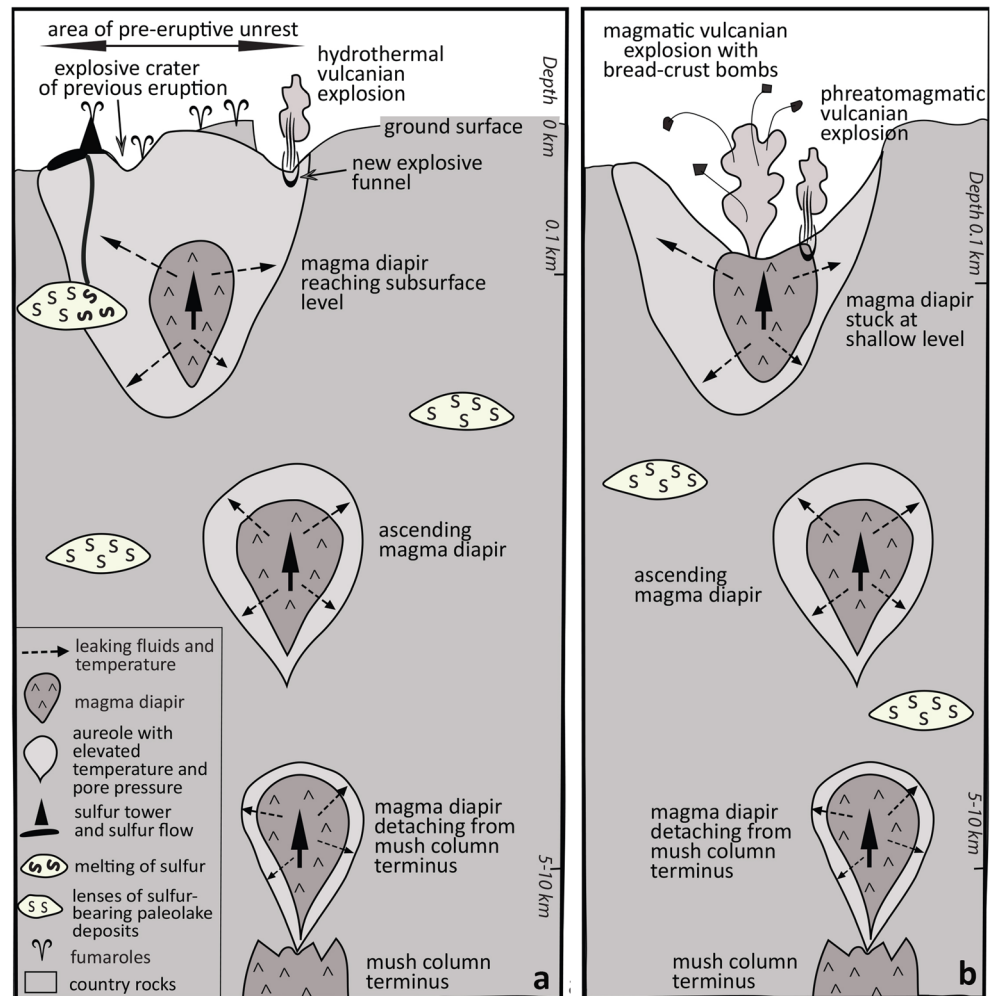
Highly crystalline, highly viscous magma that feeds eruptions of Ebeko probably ascends from the shallow (5–10 km) mush column terminus as a vertical chain of relatively small isolated magma diapirs following one another (like a sausage string) (Fig. 12). The size/volume of one diapir is equal to the volume of magma erupted during one magmatic eruption: the only estimation of the erupted volume of magma was made for the 1934–1935 eruption period, it was evaluated as about 10^6 t (Tanakadate 1936) that comprises by volume about 3×10^{-4} km³. This is the volume of spherical diapir with the radius of about 40 m. The real diapir probably has strongly elongated shape, thus its diameter should be less than 40 m. The diapirs probably form and ascend by the mechanisms similar to those of salt diapirs: many mechanisms were suggested including buoyancy (Lord 2015). Formation of such magma diapirs and diapir strings, ascending from peripheral parts of magma chambers, seems rather common: flank domes of volcanoes Bezymianny, Shiveluch, Avacha at Kamchatka (Russia) were probably formed by such diapirs. The diapirs ascend slowly, through water-saturated, fractured/fragmented hydrothermally altered country rocks, preferably along faults. The slowly ascending diapirs produce no intensive seismicity and weak ground deformations.

Pre-eruption unrest and superficial diapir ascent

While the diapirs slowly ascend, their magma gradually vesiculates/degasses, cools, and crystallizes, and the exsolved volatiles and thermal energy leek into the country rocks surrounding each diapir, where an aureole with anomalous parameters (elevated temperature, pore pressure, gas/water composition, etc.) forms. When the first magma diapir of the "sausage string" approaches the shallow subsurface level (Fig. 12a), its aureole with anomalous properties reaches the ground surface in the area above the magma diapir. At this moment, a period of pre-eruption unrest starts: the temperature of fumaroles and thermal springs increases and their compositions change. Also in few cases, surface deformations occur and fractures open (Tanakadate 1936, Kotenko et al. 2007). The elevated temperature may cause melting of native sulfur dispersed in some of the country rocks surrounding the rising magma diapir (e.g., in the lenses of buried sulfur-bearing deposits of paleocrater lakes). This sulfur pours out into the ground surface and burns, producing extensive clouds of sulfuric gases, which commonly precede and accompany eruptions of Ebeko.

Then, at some threshold, the perturbation/activation of the shallow hydrothermal system leads to initiation of phreatic/hydrothermal explosions in the area above the diapir. Vents

Fig. 12 Sketch of the “sausage string” functional model of Ebeko volcano. **a** Pre-eruption unrest. **b** Magmatic vulcanian eruption



(explosive funnels) of these explosions open in a wide area above the shallow-laying magma diapor. The exact vent locations are probably linked to the existing pathways of migrations of the hydrothermal fluids (e.g., fractured zones and diatrema-like structures of the previous eruptions). These phreatic/hydrothermal explosions tend to occur in the lowermost points/depressions of the summit area (former craters, which are located at the shortest distance from the magma diapor laying below).

Explosive activity of each magmatic eruption evolves with time from initial phreatic/hydrothermal explosions (during the period of unrest) to phreatomagmatic and then to magmatic. When the magma diapor reaches very shallow levels (at Ebeko, the depth is ~100 m), at first, the hydrothermal and phreatic explosions commence (due to heating and disturbance of the shallow geothermal system), which eject fragmented old country rocks, then phreatomagmatic explosions commence that eject both fresh fragmented magma and fragmented country rocks. These initial explosions gradually excavate a new crater down to the level of groundwater/magma interaction: this is why the craters of Ebeko are

maar-like, about 100 m deep, carved into pre-existing rocks with steep inner walls shaped by inward landslides (Auer et al. 2007). At some point, the shallow aquifer is depleted/exhausted, phreatomagmatic explosions cease, magma reaches and breaches the bottom of the new crater, and a magmatic stage of the eruption starts (Fig. 12b).

Arrival of the first magma diapor of the diapor chain at the surface marks the onset of a new series of Vulcanian magmatic explosions composing (together with the accompanying phreatic and phreatomagmatic Vulcanian explosions) one magmatic eruption of Ebeko (Fig. 12b). Arrival of the next magma diapor to the ground surface marks the onset of the next magmatic eruption. Magma diapirs in the rising string of diapirs are not necessary axially symmetric, but may have some offsets from the chain axis (these offsets probably form when the diapirs ascend through the shallow faulted crust having a complex, chaotic structure). This is the reason why active craters of Ebeko slightly change their positions from eruption to eruption and overlap at the surface. A large NNE-trending structural trend that goes along the crest of Vernadsky Ridge probably controls both the shape and

position of the small shallow crustal magma chamber/mush column of Ebeko (the shape of which probably resembles a thick NNE-trending dike), as well as the ascending path of the magma diapirs (this is why the chain of Ebeko's craters is also aligned NNE). Similar feeding systems may be common for other small-volume volcanoes composed of multiple, widely scattered eruptive centers of intermediate composition as observed at Dukono in Halmahera, Indonesia (Bani et al. 2018); the Chaîne des Puys, France (Miallier et al. 2004); Mount Usu, Japan (Goto et al. 2004); and Tongariro, New Zealand (Pardo et al. 2014).

Magma diapir breaching the ground surface boundary

“Fishing float” mechanism of a lava dome formation and the associated Vulcanian eruptions Why no new lava domes and lava flows form at Ebeko, and why few lava flows and only small domes have been formed throughout its eruptive history?

During the second (magmatic) part of the ongoing eruption of Ebeko, we have observed a nearly precise balance/equilibrium between the volume of magma that extrudes at the ground surface and the volume that is fragmented by Vulcanian explosions and carried away in the form of pyroclasts of various sizes. This balance lasts already more than 1 year, since magma reached the ground surface, and no significant morphological changes occur in the crater: no intracrater lava dome formation as well as no notable deepening of the crater floor.

The main driving force for the magma diapir ascent is probably its positive buoyancy, which is rather small in the case of Ebeko because the magma/country rock density contrast is not high. Thus, when the magma diapir breaches the ground surface, it can form a subaerial dome whose height is related to its positive buoyancy and thus its weight in the air. This is similar to what happens with a half-submerged fishing float. Further ascent/extrusion of magma becomes possible only if some weight of the subaerial part of the growing dome will be removed. Currently, at Ebeko, such removal occurs by means of Vulcanian explosive activity.

Vulcanian explosive activity is caused by violent degassing of magma due to its decompression facilitated by reduction of the litho/hydrostatic pressure when the diapir breaches the ground surface. Thus, a positive feedback loop appears: each Vulcanian explosion removes part of the dome/diapir material, which reduces its weight and allows the diapir to extrude one step higher (again only to the level where its weight will equalize its positive buoyancy), the corresponding reduction of lithostatic pressure provokes further explosive activity that in turn reduces the weight of the exposed part of the magma diapir/dome and so on. Thus, explosive activity steadily continues until the whole volume of the diapir's magma is erupted

and dispersed by the accompanying explosive Vulcanian activity.

Then some hiatus in the magmatic explosive activity starts until the moment when the next/following from below diapir reaches the shallow level and the process repeats itself (at Ebeko, we call this a new magmatic eruption). If magma of the rising diapir is too degassed and crystallized (due to, e.g., too long time of the diapir ascent) and not able to produce vulcanian explosive activity, the diapir will be extruded upward to a small height necessary to balance its positive buoyancy and then it will stall/stuck near the ground level. Reduction of the height of the extruding diapir can also occur in the form of a lava flow, but only if the viscosity of the extruding magma will allow it to flow out.

Such as magma diapirs ascend slowly at Ebeko, they arrive to the ground surface as strongly degassed and very viscous magma bodies. It explains why lava flows and strong explosive Plinian eruptions do not occur at Ebeko. The cooling and degassing of the diapirs stuck at shallow depths explain the overall high hydrothermal activity in the summit area of the volcano.

Future eruptions of Ebeko

During its eruptive history, Ebeko produced only small-volume eruptions, and thus, a large-volume future eruption of this volcano is of low probability. Eruptions of Ebeko for the last 100 years demonstrate very uniform eruption scenarios, and future eruptions of Ebeko probably will repeat, in general, the currently observed activity. Different scenarios are possible if the next rising magma diapir will reach the surface in less degassed and/or less viscous state. In this case, the future eruption can be more explosive than usual and/or can produce block lava flow, as happened last time according to Melekestsev et al. (1994) about 2000 years ago.

Because Ebeko has no prominent volcanic edifice, a large-volume gravitational flank collapse is of low probability. However, shallow-sitting collapses of superficial hydrothermally altered rocks are highly probable at its upper slopes. Such relatively small collapse can be triggered by shallow subsurface emplacement of a magma diapir. In this case, even a low-volume debris avalanche and/or the associated lahars can easily reach the town of Severo-Kurilsk. Even a small collapse can provoke intensification of explosive activity of the volcano with formation of various PDCs, which also can potentially reach the town. Lahars, caused by the eruptions, especially in winter time, are also of high probability.

Predictions of future eruptions of Ebeko are possible if modern monitoring equipment for seismicity and ground deformations of the crater area of the volcano will be installed. Monitoring of the volcano activity, gas/water geochemistry, and temperature fluctuations in the crater area are very useful and should be continued.

Conclusions

Vulcanian explosions of Ebeko (as well as Vulcanian explosions in general), although visually very similar to each other, have diverse mechanisms ranging from purely magmatic to phreatomagmatic, and to phreatic/hydrothermal. Ebeko is a relatively easily accessible volcano producing frequent explosions—it is an ideal volcano to study mechanisms of Vulcanian eruptions.

We suggest that Vulcanian eruptions of Ebeko are fed by relatively small diapirs of andesitic magma that slowly ascend through the upper crust. Such feeding systems may be common for volcanic complexes composed of multiple, widely scattered small-volume eruptive centers of intermediate composition, e.g., Dukono in Halmahera, Indonesia (Bani et al. 2018); Tongariro in New Zealand (Pardo et al. 2014); or Chaîne des Puys, France (Miallier et al. 2004). Future studies would be needed to substantiate the diapir hypothesis.

The hydrothermal system of Ebeko, despite its apparent vigor, is superficial, has a small volume, and probably is not linked to a deep source of heat. Thus, it cannot be used as a source of high-enthalpy steam to feed a power plant.

The town Severo-Kurilsk is located in a dangerous place; it can be engulfed by various types of lahars and PDCs generated by future eruptions of Ebeko. A plan for relocation of the town and construction of lahar-caching “Sabo dam” structure as well as installation of modern volcano-monitoring and lahar-warning systems is urgently necessary.

Supplementary Information The online version contains supplementary material available at <https://doi.org/10.1007/s00445-020-01426-z>.

Acknowledgments This is a contribution to VOLCAPSE, a research project funded by the European Research Council under the European Union’s H2020 Programme/ERC consolidator grant n. [ERC-CoG 646858]. Funding to Tatyana Kotenko was provided by Russian Foundation for Basic Research (RFBR), grant #20-05-00517\20. Svetlana Moskaleva, Institute of Volcanology and Seismology, assisted our SEM investigation of surface morphology of the ash particles. Atsushi Kamei, Shimane University, helped with the XRF analysis. We appreciate the help of Oleg Stuchinsky and of the staff of the seismic observatory of Russian Geophysical Survey in Severo-Kurilsk during our field work at Ebeko. Reviews of Karoly Nemeth and the anonymous reviewer were very helpful. Special thanks to BV Editors Nicole Metrich, Frances van Wyk de Vries and Jacopo Taddeucci who made great efforts in improving of our paper. This paper was written while the authors enjoyed the COVID 19 selfisolation.

References

- Annen C, Blundy JD, Sparks RSJ (2006) The genesis of intermediate and silicic magmas in deep crustal hot zones. *J Petrol* 47:505–539. <https://doi.org/10.1093/petrology/egi084>
- Auer A, Martin U, Németh K (2007) The Fekete-hegy (Balaton Highland Hungary) “soft-substrate” and “hard-substrate” maar volcanoes in an aligned volcanic complex—implications for vent geometry, sub-surface stratigraphy and the palaeoenvironmental setting. *J Volcanol Geotherm Res* 159(1–3):225–245. <https://doi.org/10.1016/j.jvolgeores.2006.06.008>
- Auer A, White JDL, Nakagawa M, Rosenberg MD (2013) Petrological record from young Ruapehu eruptions in the 4.5 ka Kiwikiwi Formation, Whangaehu Gorge, New Zealand. *N Z J Geol Geophys* 56:121–133. <https://doi.org/10.1080/00288306.2013.796998>
- Auer A, White JDL, Tobin MJ (2016) Variable H₂O content in magmas from the Tongariro Volcanic Centre and its relation to crustal storage and magma ascent. *J Volcanol Geotherm Res* 325:203–210. <https://doi.org/10.1016/j.jvolgeores.2016.06.021>
- Bani P, Tamburello G, Rose-Koga EF, Liuzzo M, Aiuppa A, Cluzel N, Amat I, Syahbana DK, Gunawan H, Bitetto M (2018) Dukono, the predominant source of volcanic degassing in Indonesia, sustained by a depleted Indian-MORB. *Bull Volcanol* 80:5. <https://doi.org/10.1007/s00445-017-1178-9>
- Basharina LA, Khramova GG (1971) Activity of Ebeko volcano in 1966–1967. *Bulletin of Volcanological Stations* 47:44–51 (in Russian)
- Chibisova MV, Degterev AV (2019) Activity of volcanoes at Kurile islands in 2018. *Bulletin of Kamchatka regional association «educational-scientific center»*. *Earth Science* 41:91–98 (in Russian). <https://doi.org/10.31431/1816-5524-2019-1-41-91-98>
- Clarke A, Ongaro TE, Belousov A (2015) Vulcanian explosions. In: Sigurdsson H et al (eds) *The encyclopedia of volcanoes*. Elsevier, Amsterdam, pp 505–518. <https://doi.org/10.1016/B978-0-12-385938-9.00028-6>
- Danyushevsky LV, Della-Pasqua FN, Sokolov S (2000) Re-equilibration of melt inclusions trapped by magnesian olivine phenocrysts from subduction-related magmas: petrological implications. *Contrib Mineral Petrol* 138:68–83. <https://doi.org/10.1007/PL00007664>
- Diller K, Clarke AB, Voight B, Neri A (2006) Mechanisms of conduit plug formation: implications for Vulcanian explosions. *Geophys Res Lett* 33:20–134. <https://doi.org/10.1016/j.epsl.2008.03.038>
- Druitt TH, Young SR, Baptie B, Bonadonna C, Calder ES, Clarke AB, Cole PD, Harford CL, Herd RA, Luckett R, Ryan G (2002) Episodes of cyclic Vulcanian explosive activity with fountain collapse at Soufrière Hills Volcano. *Montserrat Memoirs Geol Soc London* 21:281–306
- Gill J (1981) *Orogenic Andesites and plate tectonics*. Springer, Berlin
- Giordano D, Russell JK, Dingwell DB (2008) Viscosity of magmatic liquids: a model. *Earth Planet Sci Lett* 271:123–134. <https://doi.org/10.1016/j.epsl.2008.03.038>
- Gorshkov GS (1948) Names of volcanoes at Kurile Islands. *Proceedings Geograph Soc* 80:173–177 (in Russian)
- Gorshkov GS (1958) Kurile Islands. Catalog of active volcanoes of the world and Solfatara fields. Rome, IAVCEI 7:1–99
- Gorshkov GS (1970) Volcanism and the upper mantle: investigations in the Kurile Island Arc. Plenum Press 385, New York-London
- Goto Y, Ito Y, Yokoyama Y, Matsui T, Mimatsu S (2004) Internal structures of a subaerial dacite cryptodome at Usu volcano, Hokkaido, Japan. *Mem. Muroan Inst. Tech* 54(3):10. <https://doi.org/10.3389/feart.2019.00066>
- Heiken G, Wohletz K (1985) *Volcanic ash*. University Presses of California, Chicago, Harvard & MIT 246p. <https://doi.org/10.1017/S0016756800033719>
- Hoblitt RP, Harmon RS (1993) Bimodal density distribution of cryptodomed dacite from the 1980 eruption of Mount St. Helens, Washington. *Bull Volcanol* 55(6):421–437. <https://doi.org/10.1007/BF00302002>
- Houghton BF, Wilson CJN (1989) A vesicularity index for pyroclastic deposits. *Bull Volcanol* 51(6):451–462. <https://doi.org/10.1007/BF01078811>

- Kabrna P (2007) John Milne: the man who mapped the shaking Earth. Craven & Pendle Geological Society, Barnoldswick
- Kalacheva E, Taran Y, Kotenko T, Hattori K, Kotenko L, Solis-Pichardo G (2016) Volcano–hydrothermal system of Ebeko volcano, Paramushir, Kuril Islands: geochemistry and solute fluxes of magmatic chlorine and sulfur. *J Volcanol Geotherm Res* 310:118–131. <https://doi.org/10.1016/j.jvolgeores.2015.11.006>
- Kendrick JE, Lavallée Y, Varley NR, Wadsworth FB, Lamb OD, Vasseur J (2016) Blowing off steam: tuffisite formation as a regulator for lava dome eruptions. *Front Earth Sci* 4:41. <https://doi.org/10.3389/feart.2016.00041>
- Khramova GG (1987) Dynamics of formation of deposits in the crater lakes (on the case of Ebeko volcano), Vladivostok, 136 p (in Russian)
- Kimura J, Yamada Y (1996) Evaluation of major and trace element XRF analyses using a flux to sample ratio of two to one glass beads. *J Mineral Petrol Econ Geol* 91:62–72. <https://doi.org/10.2465/ganko.91.62>
- Kotenko TA, Kotenko LV, Sandimirova EI (2010) The eruption of Ebeko Volcano in January–June 2009 (Paramushir Island, Kuril Islands). Bulletin of Kamchatka regional association educational-scientific center. *Earth Sci* 15:56–68 (in Russian)
- Kotenko TA, Kotenko LV, Shapar VN (2007) Increased activity on Ebeko Volcano, Paramushir Island, North Kurils in 2005–2006. *Vulcanol Seismol* 5:3–13. <https://doi.org/10.1134/S0742046307050016>
- Kotenko TA, Kotenko LV, Sandimirova EI, Shapar VN, Timofeeva IF (2012) Eruption activity of Ebeko volcano in 2010–2011 (Paramushir Island). Bulletin of Kamchatka Regional Association <educational-scientific center>. *Earth Sci* 19:160–167 (in Russian)
- Kotenko TA, Sandimirova EI, Kotenko LV (2018) The 2016–2017 eruption of Ebeko Volcano (Kuril Islands). Bulletin of Kamchatka regional association <educational-scientific center>. *Earth Sci* 37:32–42 (in Russian)
- Kotenko TA, Sandimirova EI, Kotenko LV (2019) Eruption of Ebeko Volcano (Paramushir Island) in 2018. Conference “volcanism and connected processes”, Petropavlovsk-Kamchatsky, pp 82–85 (in Russian)
- Kotenko TA, Smirnov SZ, Sandimirova EI (2020) Dynamics of eruption of Ebeko Volcano in 2019. Conference “volcanism and connected processes”, Petropavlovsk-Kamchatsky, pp 38–41 (in Russian)
- Lange RA, Frey HM, Hector J (2009) A thermodynamic model for the plagioclase-liquid hygrometer/thermometer. *Am Mineral* 94:494–506. <https://doi.org/10.2138/am.2009.3011>
- Lautze NC, Houghton BF (2007) Linking variable explosion style and magma textures during 2002 at Stromboli volcano, Italy. *Bull Volcanol* 69:445–460. <https://doi.org/10.1007/s00445-006-0086-1>
- Le Losq C, Neuville DR, Moretti R et al (2015) Rheology of phonolitic magmas - the case of the Erebus lava lake. *Earth Planet Sci Lett* 411: 53–61. <https://doi.org/10.1016/j.epsl.2014.11.042>
- Lord AC (2015) Diapirs and salt domes. The mechanism of formation. Sandia National Lab (SNL-NM), Albuquerque United States
- Maccaferri F, Smittarello D, Pinel V, Cayol V (2019) On the propagation path of magma-filled dikes and hydrofractures: the competition between external stress, internal pressure, and crack length. *Geochem Geophys Geosyst* 20(4):2064–2081. <https://doi.org/10.1029/2018GC007915>
- Melekestsev IV, Dvigalo VN, Kir'yanov VY, Kurbatov AV, Nesmachnyi IA (1994) Ebeko volcano (Kuril Islands): history of eruption activity and future volcanic hazard. Part 2. *Vulcanol Seismol* 15(4):411–430
- Menyailov IA, Nikitina LP, Khramova GG (1969) Gas-hydrothermal eruption of Ebeko volcano in February–April 1967. *Bull Volcanol Stat* 45:3–6
- Menyailov IA, Nikitina LP, Shapar VN (1985) Results of geochemical monitoring of the activity of Ebeko volcano (Kuril Islands) used for eruption prediction. *J Geodyn* 3–4:259–274. [https://doi.org/10.1016/0264-3707\(85\)90038-9](https://doi.org/10.1016/0264-3707(85)90038-9)
- Menyailov IA, Ovsyannikov AA, Shirokov VA (1990) Eruption of Ebeko volcano in October–December 1987. *Vulcanol Seismol* 10: 493–498
- Menyailov IA, Nikitina LP, Budnikov VA (1992) Activity of Ebeko volcano in 1987–1991: style of eruptions, characteristics of their products and hazard for Severo-Kurilsk town. *Vulcanol Seismol* 5:6
- Mercalli G, Silvestri O (1891) Le eruzioni dell'Isola di Vulcano incominciate il 3 agosto 1888 e terminate il 22 marzo 1890, relazione scientifica. *Ann Ufficio Centrale Metereol Geodin Ital* 10:1–213
- Métrich N, Bertagnini A, Garaebiti E, Vergnolle S, Bani P, Beaumais A, Neuville DR (2016) Magma transfer and degassing budget: application to the 2009–2010 eruptive crisis of Mt Garet (Vanuatu arc). *J Volcanol Geotherm Res* 322:48–62. <https://doi.org/10.1016/j.jvolgeores.2015.06.003>
- Miallier D, Michon L, Évin J, Pilleyre T, Sanzelle S, Vemet G (2004) Volcans de la chaîne des Puys (Massif central, France): point sur la chronologie Vasset–Kilian–Pariou–Chopine. *Compt Rendus Geosci* 15:1345–1353. <https://doi.org/10.1016/j.crte.2004.08.002>
- Morrisey M, Mastin L (2000) Vulcanian eruptions. In: Sigurdsson H et al (eds) *The encyclopedia of volcanoes*. Elsevier, Amsterdam, pp 463–475
- Miyashiro A (1974) Volcanic rock series in island arcs and active continental margins. *Am J Sci* 274:321–355. <https://doi.org/10.2475/ajs.274.4.321>
- Mueller S, Scheu B, Kueppers U, Spieler O, Richard D, Dingwell D (2011) The porosity of pyroclasts as an indicator of volcanic explosivity. *J Volcanol Geotherm Res* 203(3–4):168–174. <https://doi.org/10.1016/j.jvolgeores.2011.04.006>
- Nakamura M, Shimakita S (1998) Dissolution origin and syn-entrapment compositional change of melt inclusion in plagioclase. *Earth Planet Sci Lett* 161:119–133. [https://doi.org/10.1016/s0012-821x\(98\)00144-7](https://doi.org/10.1016/s0012-821x(98)00144-7)
- Neave DA, Putirka KD (2017) A new clinopyroxene-liquid barometer, and implications for magma storage pressures under Icelandic rift zones. *Am Mineral* 102:777–794. <https://doi.org/10.2138/am-2017-5968>
- Németh K, Kósik S (2020) Review of explosive hydrovolcanism. *Geosciences* 10(2):44. <https://doi.org/10.3390/geosciences10020044>
- Ozerov AY, Ariskin AA, Kyle P et al (1997) Petrological–geochemical model for genetic relationships between basaltic and andesitic magmatism of Klyuchevskoi and Bezmyanni volcanoes, Kamchatka. *Petrology* 5:550–569
- Panin GL, Gora MP, Bortnikova SP, Shevko EP (2015) Subsurface structure of the northeastern fumarole field of the Ebeko volcano (Paramushir Island) according to the data of geoelectrical and geochemical studies. *Russ J Pac Geol* 9:301–311. <https://doi.org/10.1134/S1819714015040077>
- Pardo N, Cronin SJ, Németh K, Brenna M, Schipper CI, Breard E, White JD, Procter J, Stewart B, Agustín-Flores J, Moebis A (2014) Perils in distinguishing phreatic from phreatomagmatic ash; insights into the eruption mechanisms of the 6 August 2012 Mt. Tongariro eruption, New Zealand. *J Volcanol Geotherm Res* 286:397–414. <https://doi.org/10.1016/j.jvolgeores.2014.05.001>
- Putirka KD (2008) Thermometers and barometers for volcanic systems. In: Putirka KD, Tepley FJ (eds) *Minerals, inclusions and volcanic processes*. Mineralogical Soc Amer, vol 69, pp 61–120. <https://doi.org/10.2138/rmg.2008.69.3>
- Savarensky EF, Tischenko VG, Svyatlovsky AE, Dobrovol'sky AD, Zhivago AV (1958) The tsunami of 4–5 November 1952. *Bull Council Seismology Acad Sci USSR* 4:1–60 (in Russian)
- Schmincke HU (1977) Phreatomagmatische Phasen in quartären Vulkanen der Ostseifel. *Geol Jahrb* 39:3–45

- Shevko EP, Bortnikova SB, Abrosimova NA, Kamenetsky VS, Bortnikova SP, Panin GL, Zelenski M (2018) Trace elements and minerals in fumarolic sulfur: the case of Ebeko Volcano. *Kuriles Geofluids* 2018:1–16. <https://doi.org/10.1155/2018/4586363>
- Sidorov S (1966) Activization of Ebeko volcano in 1963–1964 and evolution of hydrothermal activity of the volcano before. *Bulletin of volcanological observatories* 49:61–68
- Skripko KA, Fil'kova EM, Khramova GG (1966) The state of Ebeko Volcano in the summer of 1965. *Bull Volc Observ* 42:42–55
- Sugrobov VM, Kononov VI, Postnikov AI (2005) Estimated geothermal resources of active volcanism areas at Kamchatka and Kurile islands, pp 9–24 (in Russian)
- Tanakadate H (1936) Volcanic activity in Japan during the period between July 1934 and October 1935. *Japanese J Astr Geophys* 13:121
- Vlasov GM (1958) Deposition of sulfur on volcanoes and some problems of near surface ore formation. *Proceedings Lab Volcanol* 13:166–179
- Walker GP (1971) Grain-size characteristics of pyroclastic deposits. *J Geol* 79(6):696–714. <https://doi.org/10.1086/627699>
- Walter TR, Belousov A, Belousova M, Kotenko T, Auer A (2020) The 2019 eruption dynamics and morphology at Ebeko volcano monitored by drones and field stations. *Remote Sens* 12:1961. <https://doi.org/10.3390/rs12121961>
- Winslow H, Ruprecht P, Stelten M, Amigo A (2020) Evidence for primitive magma storage and eruption following prolonged equilibration in thickened crust. *Bull Volcanol* 82:1–24. <https://doi.org/10.1007/s00445-020-01406-3>
- Wohletz KH (1983) Mechanisms of hydrovolcanic pyroclast formation: grain-size, scanning electron microscopy, and experimental studies. *J Volcanol Geotherm Res* 17(1–4):31–63. [https://doi.org/10.1016/0377-0273\(83\)90061-6](https://doi.org/10.1016/0377-0273(83)90061-6)